July 1988

Dyadic Wavelets Energy Zero-Crossings

Stephane G. Mallat
University of Pennsylvania

Dyadic Wavelets Energy Zero-Crossings

Abstract

An important problem in signal analysis is to define a general purpose signal representation which is well adapted for developing pattern recognition algorithms. In this paper we will show that such a representation can be defined from the position of the zero-crossings and the local energy values of a dyadic wavelet decomposition. This representation is experimentally complete and admits a simple distance for pattern matching applications. It provides a multiscale decomposition of the signal and at each scale characterizes the locations of abrupt changes in the signal. We have developed a stereo matching algorithm to illustrate the application of this representation to pattern matching.

Comments

University of Pennsylvania Department of Computer and Information Science Technical Report No. MS-CIS-88-30.

Dyadic Wavelets Energy Zero Crossings

MS-CIS-88-30
GRASP LAB 140

Stephane G. Mallat

Department of Computer and Information Science
School of Engineering and Applied Science
University of Pennsylvania
Philadelphia, PA 19104-6389

July 1988

This Technical Report is an invited paper for a special issue in IEEE Transactions on Information Theory

Acknowledgements:
This work was supported in part by NSF-CER grants MCS-8219196-A02, NSF/DCR-8410771, IRI84-10413-A02, Air Foc/F49620-85-K-0018, U. S. Army grants DAA29-84-K-0061, DAA29-84-9-0027 and DARPA/ONR N00014-85-K-0807.

DYADIC WAVELETS ENERGY ZERO-CROSSINGS

STEPHANE G. MALLAT

GRASP lab, Dept of Computer and Information Science
University of Pennsylvania Philadelphia, PA 19104-6389
Net address: mallat@grasp.cis.upenn.edu.arpa

ABSTRACT

An important problem in signal analysis is to define a general purpose signal representation which is well adapted for developing pattern recognition algorithms. In this paper we will show that such a representation can be defined from the position of the zero-crossings and the local energy values of a dyadic wavelet decomposition. This representation is experimentally complete and admits a simple distance for pattern matching applications. It provides a multiscale decomposition of the signal and at each scale characterizes the locations of abrupt changes in the signal. We have developed a stereo matching algorithm to illustrate the application of this representation to pattern matching.

1. Introduction

An important problem in signal analysis is to define a general purpose signal representation which is well adapted for developing pattern recognition algorithms. We shall suppose in this paper that our signal f(x) has a finite energy

$$\int_{-\infty}^{+\infty} |f(x)|^2 \, dx < +\infty \quad <==> \quad f(x) \in \mathbf{L}^2 .$$

We are first going to analyze the properties that we expect from a transform $\mathbf{T}$ which decomposes f(x) into such a meaningful representation $\mathbf{T}f$.

- $\mathbf{T}f$ must be characterized by a set of discrete values in order to be processed by a digital computer.
- A priori, we do not want to throw away any information provided by the original signal f(x) . The representation must therefore be complete which means that $\mathbf{T}$ admits an inverse $\mathbf{T}^{-1}$ on its range.
- To be able to develop algorithms which are robust to noise, any slight perturbation of the original signal f(x) should only produce a small distortion on the representation $\mathbf{T}f$ and vice-versa. Hence, the two operators $\mathbf{T}$ and $\mathbf{T}^{-1}$ should be continuous.
- In pattern recognition we want to compare a signal with a given model. We thus need to quantify the differences between the representations $\mathbf{T}f$ and $\mathbf{T}g$ of two different signals. For this purpose, we must define a simple and non ad hoc distance $\mathbf{d}(\mathbf{T}f , \mathbf{T}g)$ which can be related to more classical metrics on functions.
- For a signal f(x) , the origin of the x axis is generally chosen arbitrarily. The representation of f(x) should not depend upon the position of this origin. The transform $\mathbf{T}$ must therefore commute with any translation operator. Let $f(x) \in \mathbf{L}^2$, if $g(x) = f(x-\tau)$, the representation $\mathbf{T}g$ should be equal to the representation $\mathbf{T}f$ translated by τ .
- Recent work in signal analysis has shown that multiscale transforms provide meaningful decomposition for interpreting the informations content of many types of signals such as images [1], seismic signals [6] and speech [12]. The signal is decomposed into a set of details which a appear at different scales. Depending upon the scale, these details will characterize different kinds of structures embedded in the signal. In image processing for example, the different structures of a complex pattern such as a tree will appear at different scales. At a fine scale, the details will provide some information about the shape of the leaves and the wood texture. At a coarser scale, these details will rather characterize the shape of the branches and the overall distributions of the leaves. A multiscale organization of the signal information will also enable us to develop efficient pattern recognition algorithms based on coarse to fine strategies. We first process the coarse structures of the signal and then refine the results by processing the finer details given the prior results derived at the coarse scales. These hierarchical algorithms are computationally very efficient.

We will see in this paper that the wavelet model provides some important mathematical tools for understanding the properties of a multiscale signal decomposition. Wavelets have been introduced by A.Grossmann and J.Morlet [8] as functions whose translates and dilates could be used for expansions of $\mathbf{L}^2$. These functions are now thoroughly studied in Mathematics [14, 11], Theoretical Physics [5] and Signal Processing [12]. We will first define mathematically a dyadic wavelet transform and describe its fundamental properties. We will then show why the more classical [4] approach for discretizing this transform does not provide a translating representation ; when a signal is translated the discrete wavelet transform of this signal is not translated but completely modified. We will thus introduce another discrete transform based on the zero-crossings and the local energy values of the dyadic wavelet decomposition. This new representation does translate when the signal translates. For any wavelet which is the second derivative of a smoothing function, the zero-crossings of a dyadic wavelet decomposition provide the locations of the abrupt changes in the signal. These abrupt modifications are meaningful features because they often correspond to the borders of the structures embedded in the signal. We will study the properties of this Energy Zero-Crossing representation and show that it is well adapted to pattern recognition applications. We will show in particular that one can reconstruct a signal from the zero-crossings and local energy values of the dyadic wavelet transform. In order to compute an Energy Zero-Crossing representation of a function, we must first compute its dyadic wavelet transform. We will describe a pyramidal algorithm of complexity n.log(n) for doing so and then show how to derive the Energy Zero-Crossing representation. We will also detail the implementation of a recursive algorithm which reconstructs the original signal from this representation. To illustrate the application of this representation in pattern matching, we have developed a stereo matching algorithm. The stereo matching problem consists of finding a point by point correspondence between two signals which are shifted from one another and have some local distortions. In image processing, we must solve such a correspondence problem when trying to recover the three dimensional shape of the surfaces which appear in a pair of stereo images.

Notations: For any pair of functions $f(x) \in \mathbf{L}^2$ and $g(x) \in \mathbf{L}^2$,

$$< g , f > = \int_{-\infty}^{+\infty} g(x) f(x)\, dx \qquad \text{will denote the inner product in } \mathbf{L}^2 \text{ and}$$

$$//f//^2 = \int_{-\infty}^{+\infty} |f(x)|^2 dx \qquad \text{will denote the norm of f(x) .} \tag{1}$$

The Fourier transform of f(x) will be written

$$\hat{f}(\omega) = \int_{-\infty}^{+\infty} f(x)\, e^{-i\omega x}\, dx \ . \tag{2}$$

We shall also denote by $f^j(x) = 2^j f(2^j x)$ the scaling of f(x) with a factor 2^j . The symmetrical of f(x)

will be written $\tilde{f}(x) = f(-x)$. The vector space $\mathbf{C}$ will denote the set of $\mathbf{L}^2$ functions which are continuous. $(\mathbf{L}^2)^{\mathbf{Z}}$ will be the vector space of all infinite sequences $\left[g_j(x)\right]_{j\in\mathbf{Z}}$ of $\mathbf{L}^2$ functions such that

$$\sum_{j\in\mathbf{Z}} \|g_j\|^2 < +\infty \quad . \tag{3}$$

This summation defines a norm on $(\mathbf{L}^2)^{\mathbf{Z}}$. Finally, $(\mathbf{L}^2)^n$ will denote the vector space of finite sequences $\left[g_j(x)\right]_{1\le j\le n}$ of $\mathbf{L}^2$ functions .

2. Dyadic Wavelet transform

2.1. Smoothing functions and wavelets

In this paragraph, we will introduce the dyadic wavelet representation as a transform which decomposes a continuous signal into a sum of details appearing at the scales $(2^j)_{j\in\mathbf{Z}}$. The dyadic wavelet transform is a discretization along the scale axis of the continuous wavelet transform defined by J. Morlet and A. Grossmann [8]. We have chosen a dyadic decomposition for simplifying the computer implementation of the transform.

Let S^j be the operator which smooths at the scale 2^j any function $f(x) \in \mathbf{L}^2$. This operator convolves f(x) with a function $\phi(x)$ scaled by a factor 2^j :

$$S^j f(x) = f * \phi^j(x) \quad . \tag{4}$$

The function $\phi(x)$ will be called a **smoothing function.** Let us first study the properties of the operator S^j and of the corresponding smoothing function $\phi(x)$. We will then show how to define the details of a function f(x) at the scale 2^j from such an operator. For normalization purposes we will impose that

$$\|\phi\| = 1 \quad . \tag{5}$$

A smoothing operation must gradually attenuate the details of a function when the scale decreases. From $S^{j+1}f(x)$ we should be able to compute $S^j f(x)$ with an additional smoothing. Let $\hat{S^j f}(\omega)$ and $\hat{S^{j+1}f}(\omega)$ be respectively the Fourier transform of $S^j f(x)$ and $S^{j+1}f(x)$. This property will be verified if and only if

$$|\hat{S^j f}(\omega)| \le |\hat{S^{j+1}f}(\omega)| \quad . \tag{6}$$

Since $\hat{S^j f}(\omega) = \hat{f}(\omega)\,\hat{\phi}(2^{-j}\omega)$ and $\hat{S^{j+1}f}(\omega) = \hat{f}(\omega)\,\hat{\phi}(2^{-j-1}\omega)$, equation (6) implies that there exists a function $H(\omega)$ such that

$$\hat{\phi}(2\omega) = H(\omega)\,\hat{\phi}(\omega) \quad \text{and} \quad \forall \omega \in \mathbf{R} \quad |H(\omega)| \le 1 \quad . \tag{7}$$

The Fourier transform of $S^j f(x)$ and $S^{j+1} f(x)$ are thus related by

$$\hat{S^j} f(\omega) = H(2^{-j-1}\omega)\, \hat{S^{j+1}} f(\omega) \ . \tag{8}$$

$H(2^{-j-1}\omega)$ is the additional smoothing which is needed in order to go from the scale 2^{j+1} to the scale 2^j . Equation (7) shows that the Fourier transform of a smoothing function can be expressed from $H(\omega)$:

$$\hat{\phi}(\omega) = \prod_{p=1}^{+\infty} H(2^{-p}\omega) \ . \tag{9}$$

When the scale increases towards plus infinity we expect that the operator S^j will attenuate less and less the function details and that $S^j f(x)$ will converge in $\mathbf{L}^2$ towards f(x) . Conversely when the scale decreases towards zero, we smooth more and more the signal details and expect that the resulting signal will ultimately converges towards zero. One can easily show that these constraints are equivalent to the following conditions on the Fourier transform of $\phi(x)$:

$$\lim_{|\omega| \to 0} \hat{\phi}(\omega) = 1 \quad \text{and} \tag{10}$$

$$\lim_{|\omega| \to +\infty} \hat{\phi}(\omega) = 0 \ . \tag{11}$$

When smoothing a signal f(x) , we do not loose any information if the Fourier transform of the smoothing function does not have any zero. It is theoretically possible to reconstruct f(x) from $S^j f(x)$ with a deconvolution but such a deconvolution procedure is unstable.

To extract the details which appear in $S^{j+1} f(x)$ but have been attenuated in $S^j f(x)$ we are going to introduce the function $\psi(x) \in \mathbf{L}^2$ whose Fourier transform is given by

$$|\hat{\psi}(\omega)|^2 = |\hat{\phi}(\frac{\omega}{2})|^2 - |\hat{\phi}(\omega)|^2 \ . \tag{12}$$

The function $\psi(x)$ is called a **dyadic wavelet.** By integrating equation (12) on ω between $-\infty$ and $+\infty$ and applying Parseval's theorem, we can show that $//\psi// = //\phi// = 1$. Since any smoothing function verifies $\hat{\phi}(\omega) = H(\frac{\omega}{2})\, \hat{\phi}(\frac{\omega}{2})$, the Fourier transform of a wavelet can also be written

$$\hat{\psi}(2\omega) = G(\omega)\, \hat{\phi}(\omega) \quad \text{where} \quad |H(\omega)|^2 + |G(\omega)|^2 = 1 \ . \tag{13}$$

With a simple summation on equation (12) we can show also that

$$\sum_{j=-J}^{J} |\hat{\psi}(2^j\omega)|^2 = |\hat{\phi}(2^{-J-1}\omega)|^2 - |\hat{\phi}(2^J\omega)|^2 \ . \tag{14}$$

By taking the limit of (14) when J tends towards $+\infty$ and applying the properties (10) and (11) of a smoothing

function, we have

$$\lim_{J\to+\infty} \sum_{j=-J}^{J} |\hat{\psi}(2^j\omega)|^2 = \sum_{j\in Z} |\hat{\psi}(2^j\omega)|^2 = 1 \quad . \tag{15}$$

This convergence is clearly uniform for $|\omega| > 1$. Lemma 1 shows that this property is a characterization of a dyadic wavelet.

Lemma 1

Any function $\psi(x) \in \mathbf{L}^2$ such that $//\psi// = 1$ is a wavelet function if and only if

$$\forall \omega \in \mathbf{R} \qquad \lim_{J\to+\infty} \sum_{j=-J}^{J} |\hat{\psi}(2^j\omega)|^2 = 1 \quad , \quad \text{and the convergence is uniform for } |\omega| \geq 1 \ .$$

Fig. 1 shows an example of a smoothing function with its Fourier transform. Fig. 2 shows the associated wavelet with its Fourier transform. These particular functions are further described in paragraph 6.1.1 .

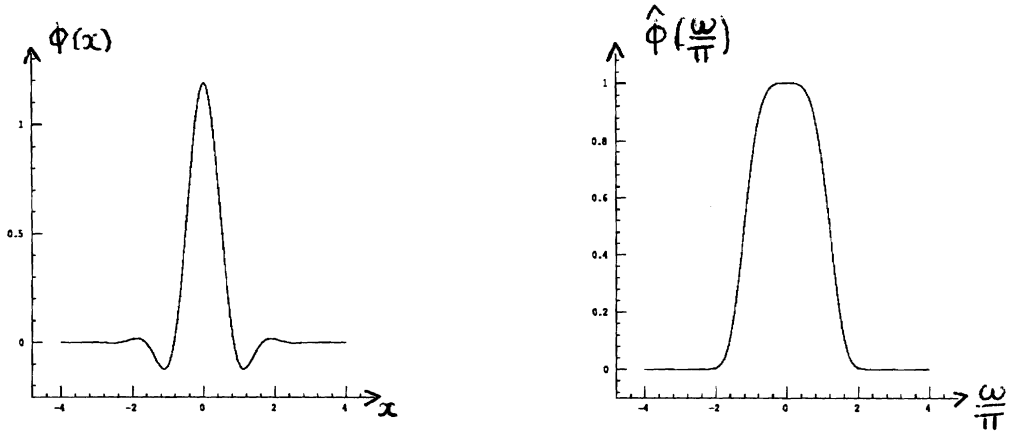

Fig. 1. *The left and right figures are respectively the graph of a smoothing function* $\phi(x)$ *and its Fourier transform* $\hat{\phi}(\frac{\omega}{\pi})$. $\phi(x)$ *is a low pass filter.*

Given a wavelet $\psi(x)$, the **wavelet transform at a scale** 2^j of $f(x) \in \mathbf{L}^2$ is defined by

$$W^j f(x) = f * \psi^j(x) \ . \tag{17}$$

The wavelet transform of f(x) at the scale 2^j provides the details of f(x) which have been attenuated between the scales 2^{j+1} and 2^j . The energy of these details are equal to the difference of the energies of $S^j f$ and $S^{j+1} f$:

$$//W^j f// = //S^{j+1} f// - //S^j f// \ . \tag{18}$$

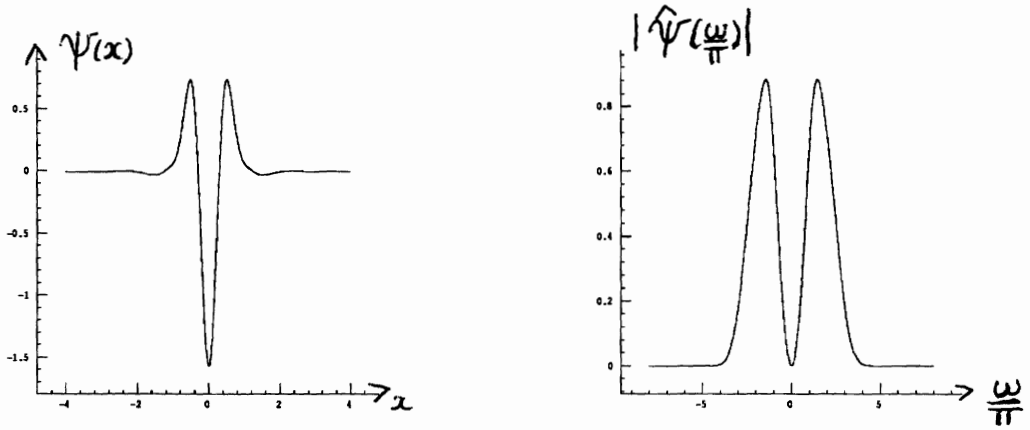

Fig. 2. *The left and right figures are respectively the graph of a wavelet* $\psi(x)$ *and the absolute value of its Fourier transform* $|\hat{\psi}(\frac{\omega}{\pi})|$. $\psi(x)$ *is a band pass filter.*

Proof of equation (18) : We can derive from equation (12) that

$$|\hat{f}(\omega)|^2 \, |\hat{\psi}(2^{-j}\omega)|^2 = |\hat{f}(\omega)|^2 \, |\phi(2^{-j-1}\omega)|^2 - |\hat{f}(\omega)|^2 \, |\phi(2^{-j}\omega)|^2 \quad .$$

By integrating this equation between $-\infty$ and $+\infty$ and applying Parseval's theorem we get equation (18) .

2.2. Infinite dyadic wavelet transform

We shall call **Infinite Dyadic Wavelet Transform** of f(x) , the sequence of functions

$$\mathbf{W_I} f = \left[W^j f(x) \right]_{j \in \mathbf{Z}} . \tag{19}$$

Such a transform decomposes a function into its details which appear at all the scales $(2^j)_{j \in \mathbf{Z}}$. We will study in this paragraph the most important properties of this transform.

• Translating property

Let $f(x) \in \mathbf{L}^2$ and $g(x) = f(x-\tau)$ be a translation of f(x) by τ . Since the convolution product is shifting,

$$W^j g(x) = W^j f(x-\tau) . \tag{20}$$

The wavelet transform of g(x) is equal to the wavelet transform of f(x) translated by τ .

• Completeness of the wavelet representation

A function can be reconstructed from its wavelet representation.

$$f(x) = \sum_{j=-\infty}^{+\infty} W^j f(x) * \tilde{\psi}^j(x) = \mathbf{W_I}^{-1} \left[W^j f(x) \right]_{j \in \mathbf{Z}} . \tag{21}$$

The inverse wavelet transform operator $\mathbf{W}_\mathbf{I}^{-1}$ is characterized by equation (21).

Proof : Multiplying equation (15) by $\hat{f}(\omega)$ gives

$$\hat{f}(\omega) = \sum_{j \in \mathbf{Z}} \hat{f}(\omega)\, |\hat{\psi}(2^j \omega)|^2 \ .$$

This expression is the Fourier transform of equation (21).

• Energy conservation

The total energy of a signal can be decomposed as a sum of the energies of the details appearing at each scale 2^j.

$$||f(x)||^2 = \sum_{j=-\infty}^{+\infty} ||W^j f(x)||^2 \ . \tag{22}$$

Proof : If we multiply equation (15) by $|\hat{f}(\omega)|^2$ we get

$$|\hat{f}(\omega)|^2 = \sum_{j \in \mathbf{Z}} |\hat{f}(\omega)|^2\, |\hat{\psi}(2^j \omega)|^2 \ .$$

By integrating this equation between $+\infty$ and $-\infty$ we obtain equation (22) .

• Continuity and dyadic wavelet transform space

Let $\mathbf{I}$ be the sub-vector space of $(\mathbf{L}^2)^\mathbf{Z}$ of all the wavelet transform $\mathbf{W}_\mathbf{I} f = \left[W^j f(x) \right]_{j \in \mathbf{Z}}$ for $f(x) \in \mathbf{L}^2$. We saw that $\mathbf{W}_\mathbf{I}$ admits an inverse $\mathbf{W}_\mathbf{I}^{-1}$ which is characterized by equation (21). The operator $\mathbf{W}_\mathbf{I}$ is thus an isomorphism from $\mathbf{L}^2$ onto $\mathbf{I}$. The energy conservation equation shows that this isomorphism is isometric for the norm on $(\mathbf{L}^2)^\mathbf{Z}$ defined by equation (3) . The operators $\mathbf{W}_\mathbf{I}$ and $\mathbf{W}_\mathbf{I}^{-1}$ are therefore continuous.

To characterize the vector space $\mathbf{I}$ we are going to build a projection operator $P_\mathbf{I}$ from $(\mathbf{L}^2)^\mathbf{Z}$ on $\mathbf{I}$. This projection operator will be defined from the wavelet transform $\mathbf{W}_\mathbf{I}$ and the inverse wavelet transform $\mathbf{W}_\mathbf{I}^{-1}$. We saw that the inverse wavelet transform $\mathbf{W}_\mathbf{I}^{-1}$ was characterized by equation (21) for any element of $\mathbf{I}$. Let us first extend the operator $\mathbf{W}_\mathbf{I}^{-1}$ to the all space $(\mathbf{L}^2)^\mathbf{Z}$:

$$\forall \left[g_j(x) \right]_{j \in \mathbf{Z}} \in (\mathbf{L}^2)^\mathbf{Z} \qquad \mathbf{W}_\mathbf{I}^{-1} \left[g_j(x) \right]_{j \in \mathbf{Z}} = \sum_{j \in \mathbf{Z}} g_j * \tilde{\psi}^j(x) \ . \tag{23}$$

One can easily show that $\mathbf{W}_\mathbf{I}^{-1} \left[g_j \right]_{j \in \mathbf{Z}} \in \mathbf{L}^2$. We can now characterize the vector space $\mathbf{I}$ with the projection operator $P_\mathbf{I}$ defined by

$$P_\mathbf{I} = \mathbf{W}_\mathbf{I} \ o \ \mathbf{W}_\mathbf{I}^{-1} \ . \tag{24}$$

$$(\mathbf{L}^2)^\mathbf{Z} \xrightarrow{\mathbf{W}_\mathbf{I}^{-1}} \mathbf{L}^2 \xrightarrow{\mathbf{W}_\mathbf{F}} \mathbf{I} \ .$$

This operator clearly verifies the conditions of a projection operator from $(\mathbf{L}^2)^{\mathbf{Z}}$ on $\mathbf{I}$:

$$\forall \left(g_j(x)\right)_{j\in\mathbf{Z}} \in (\mathbf{L}^2)^{\mathbf{Z}} \quad , \quad P_{\mathbf{I}}\left(g_j(x)\right)_{j\in\mathbf{Z}} \in \mathbf{I} \quad \text{and} \tag{25}$$

$$\left(g_j(x)\right)_{j\in\mathbf{Z}} \in \mathbf{I} \quad \text{if and only if} \quad P_{\mathbf{I}}\left(g_j(x)\right)_{j\in\mathbf{Z}} = \left(g_j(x)\right)_{j\in\mathbf{Z}} \ . \tag{26}$$

Let us insert in equation (24) the expressions of $\mathbf{W}_{\mathbf{I}}$ and $\mathbf{W}_{\mathbf{I}}^{-1}$ given by equations (17) and (21)

$$P_{\mathbf{I}}\left(g_j(x)\right)_{j\in\mathbf{Z}} = \left(\sum_{k=-\infty}^{+\infty} K_{j,k} * g_k(x)\right)_{j\in\mathbf{Z}} \quad \text{where} \quad K_{j,k}(x) = \psi^j * \tilde{\psi}^k(x) \ . \tag{27}$$

As a consequence of equation (26), for any wavelet transform $\mathbf{W}_{\mathbf{I}} f = \left(W^j\right)_{j\in\mathbf{Z}}$ we have in particular

$$\forall j \in \mathbf{Z} \quad , \quad W^j f(x) = \sum_{k=-\infty}^{+\infty} K_{j,k} * W^k f(x) \ . \tag{28}$$

This equation expresses the redundancy between the wavelet transforms at different scales. The functions $K_{j,k}(x)$ are called reproducing kernels. The concept of reproducing kernel has been introduced by A. Grossmmann and J. Morlet [8]. The correlation of the wavelet transforms $W^k f(x)$ and $W^j f(x)$ is given by the energy of the reproducing kernel $K_{j,k}(x)$.

In practice a measuring device does not measure exactly a continuous signal but only an approximation at a finite resolution r_0. A priori, we do not want to compute the dyadic wavelet transform of such an approximated signal at a scale bigger than r_0. Indeed, if the scale is finner than the resolution, the details of the measured signal do not carry any information about the original signal. In the next paragraph, we will modeled the concept of approximation at a finite resolution and describe its main properties. We will then define the finite dyadic wavelet transform of such an approximation.

2.3. Finite Dyadic Wavelet Transform

2.3.1. Modeling of a finite resolution approximation

Intuitively, the approximation of any signal at a resolution r_0 is a signal which varies smoothly over a distance $\frac{1}{r_0}$ and which can be characterized by r_0 samples per length unit. We will suppose here that the resolution r_0 varies on a dyadic sequence $(2^j)_{j\in\mathbf{Z}}$. In this paragraph, we are going to summarize the resolution model that we have developed for studying the orthogonal wavelets of Yves Meyer [17, 16]. The understanding of a finite resolution approximation will then enable us to define a finite dyadic wavelet transform.

Let us denote by A^j the operator which associates to any function $f(x) \in \mathbf{L}^2$ an approximation at the resolution 2^j. Such an operator can be characterized by the following six properties that one would intuitively expect from such an approximation.

- A^j is a linear operator. If $A^j f(x)$ is the approximation of some signal f(x) at the resolution 2^j, $A^j f(x)$ will not be modified if we approximate it at the resolution 2^j.

This principle shows that $A^j \; o \; A^j = A^j$. The operator A^j is thus a projection operator on a particular vector space $\mathbf{V}_j$ included in $\mathbf{L}^2$. $\mathbf{V}_j$ is the set of all possible approximated signals at resolution 2^j.

- Among all the approximated function at the resolution 2^j, $A^j f(x)$ is the function which is the most similar to f(x).

$$\forall g(x) \in \mathbf{V}_j \quad , \quad \|g(x) - f(x)\| \geq \|A^j f(x) - f(x)\| \quad .$$

The operator A^j is thus an orthonormal projection on the vector space $\mathbf{V}_j$.

- Causality: The approximation of a signal at resolution 2^{j+1} contains all the necessary informations to build the same signal at a smaller resolution 2^j.

Since A^j is a projection operator on $\mathbf{V}_j$ this principle is equivalent to :

$$\forall j \in \mathbf{Z}, \quad \mathbf{V}_j \subset \mathbf{V}_{j+1} . \tag{29}$$

- An approximation operation is similar at all resolutions.

The spaces of approximated functions should thus be derived from one another by scaling each approximated function by the ratio of the resolution values.

$$\forall j \in \mathbf{Z}, \quad g(x) \in \mathbf{V}_j \quad \Longleftrightarrow \quad g(2x) \in \mathbf{V}_{j+1} . \tag{30}$$

- The approximation $A^j f(x)$ of a signal f(x) can be characterized by 2^j samples per length unit. When f(x) is translated by a length proportional to 2^{-j}, $A^j f(x)$ is translated and it is characterized by the same samples which have been translated.

Because of the condition (30), it is sufficient to express the above principle for j = 0. This statement can be modeled as follow :

Discrete characterization : There exists an isomorphism I_0 from $\mathbf{V}_0$ onto $\mathbf{l}^2(\mathbf{Z})$ (31)

$$\text{where} \quad \mathbf{l}^2(\mathbf{Z}) = \{(\alpha_i)_{i \in \mathbf{Z}} \; / \; \sum_{i=-\infty}^{+\infty} |\alpha_i|^2 < +\infty\}$$

Translation of the approximation : $\forall k \in \mathbf{Z} \quad A^j(f(u-k))(x) = A^j(f(u))(x-k)$. (32)

Translation of the samples : $I_0(A^j f(x)) = (\alpha_i)_{i \in \mathbf{Z}} \iff I_0(A^j f(x-k)) = (\alpha_{i-k})_{i \in \mathbf{Z}}$. (33)

• Contrary to smoothing at a scale 2^j , when computing an approximation at a resolution 2^j we loose some information about the original signal f(x) . This lost information corresponds to the orthonormal projection of f(x) on the orthogonal complement of $\mathbf{V}_j$ in $\mathbf{L}^2$. However, when the resolution increases towards $+\infty$ the approximated signal should converge towards the original signal. Conversely when the resolution decreases to zero, the approximated signal contains less and less information and should ultimately converge towards zero.

Since the approximated signal at a resolution 2^j is equal to the orthogonal projection on a space $\mathbf{V}_j$, this principle can be written :

$$\bigcup_{j=-\infty}^{j=+\infty} \mathbf{V}_j \text{ is dense in } \mathbf{L}^2 \quad \text{and} \quad \bigcap_{j=-\infty}^{j=+\infty} \mathbf{V}_j = \{0\} \ . \tag{34}$$

We will call any set of vector spaces $\left(\mathbf{V}_j\right)_{j \in \mathbf{Z}}$ which verifies the properties (29) to (34) a **multiresolution approximation** of $\mathbf{L}^2$. In order to characterize numerically the orthonormal projection operator A^j , we must find an orthonormal basis of $\mathbf{V}_j$. The following theorem shows that such an orthonormal basis can be defined by scaling and translating a unique function $\xi(x)$.

Theorem 1

Let $\left(\mathbf{V}_j\right)_{j \in \mathbf{Z}}$ be a multiresolution approximation of $\mathbf{L}^2$. There exists a unique function $\xi(x)$ called a **scaling function** such that

$$\forall j \in \mathbf{Z} \ , \ \left(\sqrt{2^{-j}}\, \xi^j(x - 2^{-j}n)\right)_{n \in \mathbf{Z}} \text{ is an orthonormal basis of } \mathbf{V}_j \ . \tag{35}$$

We can therefore build an orthonormal basis of any $\mathbf{V}_j$ by scaling the function $\xi(x)$ with a coefficient 2^j and translating the resulting function on a grid whose interval is proportional to 2^{-j} . The factor $\sqrt{2^{-j}}$ is a normalization with respect to the $\mathbf{L}^2$ norm. We can now define the orthogonal projection operator A^j from this orthonormal basis :

$$\forall f(x) \in \mathbf{L}^2 \ , \ A^j f(x) = \sum_{n=-\infty}^{+\infty} 2^{-j} \langle f(u), \xi^j(u-2^{-j}n) \rangle \ \xi^j(x - 2^{-j}n) \ . \tag{36}$$

The vector space $\mathbf{V}_j$ of all the approximations at the resolution 2^j of $\mathbf{L}^2$ functions is characterized by :

$$\forall f^*(x) \in \mathbf{V}_j \ , \ \exists (\alpha_n) \in \mathbf{l}^2(\mathbf{Z}) \ , \ f^*(x) = \sum_{n=-\infty}^{+\infty} \alpha_n \sqrt{2^{-j}}\ \xi^j(x - 2^{-j}n) \ . \tag{37}$$

Lemma 2

Let $\left\{ \mathbf{V}_j \right\}_{j \in \mathbf{Z}}$ be a multiresolution space sequence and $\xi(x)$ be the associated scaling function. If there exist a function $\nu(x) \in \mathbf{L}^2$ such that

$$\xi(x) = \phi * \nu(x) \quad \text{with} \quad \hat{\nu}(\omega) = O(\frac{1}{\omega}) \ , \quad \text{then} \tag{38}$$

$$\forall f^*(x) \in \mathbf{V}_j \ , \ \exists f(x) \in \mathbf{L}^2 \quad \text{such that} \quad f^* = S^j f \ . \tag{39}$$

The proof of this lemma is given in appendix 2. If the scaling function $\xi(x)$ verifies the condition of the lemma, any approximated function at the resolution 2^j is thus equal to a smoothing at the scale 2^j of some function in $\mathbf{L}^2$. The contrary is false. The smoothing at the scale 2^j of any function in $\mathbf{L}^2$ is not a priori the approximation at the resolution 2^j of some function in $\mathbf{L}^2$. We show in appendix 2 that a function $f(x) \in \mathbf{L}^2$ will verify $S^j f(x) \in \mathbf{V}_j$ if and only if

$$\exists (\alpha_n)_{n \in \mathbf{Z}} \in \mathbf{l}^2(\mathbf{Z}) \ , \ f(x) = \sum_{n=-\infty}^{+\infty} \alpha_n \sqrt{2^{-j}} \ \nu^j(x - 2^{-j} n) \ . \tag{40}$$

The function $f(x)$ must therefore be in the vector space generated by the family of functions $\left\{ \nu^j(x - 2^{-j} n) \right\}_{n \in \mathbf{Z}}$; it can not be any function in $\mathbf{L}^2$.

A multiresolution approximation $\left\{ \mathbf{V}_j \right\}_{j \in \mathbf{Z}}$ is completely characterized by the corresponding scaling function $\xi(x)$. Conversely, we will call a scaling function any function $\xi(x) \in \mathbf{L}^2$ such that , for all $j \in \mathbf{Z}$, $\left\{ \sqrt{2^{-j}} \ \xi^j(x - 2^{-j} n) \right\}_{n \in \mathbf{Z}}$ is an orthonormal family and if $\mathbf{V}_j$ is the vector space generated by this family of functions, then $\left\{ \mathbf{V}_j \right\}_{j \in \mathbf{Z}}$ is a multiresolution approximation of $\mathbf{L}^2$. The following theorem gives a practical characterization of the Fourier transform of a scaling function.

Theorem 2

Let $\xi(x)$ be a scaling function and $X(\omega)$ be the 2π periodic function defined by :

$$X(\omega) = \sum_{n=-\infty}^{+\infty} <\sqrt{2^{-1}}\,\xi(\tfrac{u}{2}) , \xi(u-n) > e^{-in\omega} . \tag{41}$$

The function $X(\omega)$ verifies the following properties :

(a) $|X(0)| = 1$.

(b) $|X(\omega)|^2 + |X(\omega+\pi)|^2 = 1$

Conversely let $X(\omega)$ be a 2π periodic function satisfying (a) , (b) and such that

(c) $|X(\omega)| \neq 0$ for $\omega \in [0 , \pi/2]$

$$\text{then,} \quad \hat{\xi}(\omega) = \prod_{p=1}^{+\infty} X(2^{-p}\omega) \quad \text{is the Fourier transform of a scaling function .} \tag{42}$$

The proof of this theorem can be found in [17]. It is not difficult to defined numerically a function $X(\omega)$ which verifies the properties (a) , (b) and (c) . With equation (12) we will thus be able to compute the Fourier transform $\hat{\xi}(\omega)$ of some scaling functions and hence the scaling function $\xi(x)$ itself with an inverse Fourier transform.

A convenient characterization of a signal approximated at the resolution 2^j is to uniformly sample this signal at the rate 2^j . The following theorem shows how to reconstruct an approximation $A^j f(x)$ from the set of samples $\left[A^j f(2^{-j}n)\right]_{n\in\mathbf{Z}}$.

Theorem 3

If there exist two constants c_1 and c_2 such that $c_1 \leq \sum_{n=-\infty}^{+\infty} \hat{\xi}(\omega+2n\pi) \leq c_2$, then any function $f(x) \in \mathbf{V}_j$ can be decomposed into

$$f(x) = \sum_{n=-\infty}^{+\infty} f(2^{-j}n)\, 2^{-j}\, \rho^j(x - 2^{-j}n) . \tag{43}$$

The spline function $\rho(x)$ is unique and its Fourier transform is given by

$$\hat{\rho}(\omega) = \frac{\hat{\xi}(\omega)}{\sum_{n=-\infty}^{+\infty} \hat{\xi}(\omega+2n\pi)} . \tag{44}$$

The proof of this lemma is detailed in appendix 3. In general, we will characterize a signal approximated at the resolution 2^j by providing a uniform sampling of this signal.

Let us suppose that we have been able to approximate a function f(x) at the resolution 2^{j_2}. This approximation $A^{j_2}f(x)$ does not contain any information on the details of the function which are smaller than 2^{-j_2}. It would thus be absurd to try to compute the wavelet transform of this approximated function for any scale bigger than 2^{j_2}. In the next paragraph we will study a finite dyadic wavelet transform of such an approximated function.

2.3.2. Definition and properties of a finite dyadic wavelet transform

We will suppose in this paragraph that we can only recover an approximation at the resolution 2^{j_2} of the original function. The resolution 2^{j_2} can be viewed as the maximum resolution of our measuring device. We will also suppose that the scaling function $\xi(x)$ verifies the condition of lemma 2. The approximation at the resolution 2^{j_2} of any function in $f^*(x) \in \mathbf{V}_{j_2}$ can thus be interpreted as a smoothing at a scale 2^{j_2} of some function $f(x) \in \mathbf{L}^2 : f^*(x) = S^j f(x)$. We want to emphasize once more that the contrary is not true. From now on, we will denote by $f^*(x) = S^{j_2}f(x) \in \mathbf{V}_{j_2}$ any approximated function at the resolution 2^{j_2}. The incremental smoothing property (6) implies that from $S^{j_2}f(x)$ we can compute the wavelet transform of f(x) at any smaller scale 2^j, $j < j_2$. In practical computations we must however stop the wavelet decomposition at some finite resolution 2^{j_1}.

We shall call **finite dyadic wavelet transform** between the scale 2^{j_2} and 2^{j_1} the operator $\mathbf{W_F}$ which transforms any function $S^{j_2}f \in \mathbf{V}_{j_2}$ into the set of functions

$$\mathbf{W_F}(S^{j_2}f) = \left\{ \left[W^j f(x) \right]_{j_1 \le j < j_2} , S^{j_1} f(x) \right\} \quad . \tag{45}$$

It provides a smoothing of the signal f(x) at a coarse scale 2^{j_1} plus the successive details which appear between the scales 2^{j_1} and 2^{j_2}. Let $(\mathbf{L}^2)^{j_2-j_1}$ be the set of finite sequence of $\mathbf{L}^2$ functions $\left[g_j(x) \right]_{j_1-1 \le j < j_2}$. The operator $\mathbf{W_F}$ transforms any approximated signal $f^* = S^j f \in \mathbf{V}_{j_2}$ into an element of $(\mathbf{L}^2)^{j_2-j_1}$.

• Computation of a finite dyadic wavelet transform

We are going to describe a simple pyramidal algorithm for computing a finite dyadic wavelet transform for any approximated signal $S^{j_2}f \in \mathbf{V}_{j_2}$. We saw in paragraph 2.1 that the Fourier transforms of a smoothing function and its associated wavelet verify

$$\hat{\phi}(\omega) = H(\tfrac{\omega}{2})\, \hat{\phi}(\tfrac{\omega}{2}) \quad \text{and} \quad \hat{\psi}(\omega) = G(\tfrac{\omega}{2})\, \hat{\phi}(\tfrac{\omega}{2}) \quad .$$

At any scale 2^j, the Fourier transform of $S^{j+1}f(x)$, $S^jf(x)$ and $W^jf(x)$ are thus related by

$$\hat{S}^jf(\omega) = \hat{f}(\omega)\,\hat{\phi}(2^{-j}\omega) = \hat{f}(\omega)\,H(2^{-j-1}\omega)\,\hat{\phi}(2^{-j-1}\omega) = H(2^{-j-1}\omega)\,\hat{S}^{j+1}f(\omega) \quad \text{and} \tag{46}$$

$$\hat{W}^jf(\omega) = \hat{f}(\omega)\,\hat{\psi}(2^{-j}\omega) = \hat{f}(\omega)\,G(2^{-j-1}\omega)\,\hat{\phi}(2^{-j-1}\omega) = G(2^{-j-1}\omega)\,\hat{S}^{j+1}f(\omega) \ . \tag{47}$$

Since $|H(\omega)| \leq 1$ and $|G(\omega)| \leq 1$, we can define the inverse Fourier transform of these functions in the sense of Schwartz distributions. Let h^j and g^j be the inverse Fourier transform of $H(2^{-j}\omega)$ and $G(2^{-j}\omega)$. Equation (46) and (47) yield

$$S^jf(x) = S^{j+1}f * h^{j+1} \quad \text{and} \tag{48}$$

$$W^jf(x) = S^{j+1}f * g^{j+1} \ . \tag{49}$$

By iterating on these two equations when j goes from $j_2 - 1$ to j_1 , we can compute the finite dyadic wavelet transform of $S^{j_2}f(x)$.

In all the examples which will be shown, we will suppose that the input signal was measured at the resolution 1 . The maximum scale 2^{j_2} of the finite dyadic wavelet transforms will thus be equal to 1 ($j_2 = 0$) . Fig 3 shows an example of a signal approximated at the resolution 1 and Fig. 4 gives a finite dyadic wavelet decomposition between the scales 1 and 2^{-5} ($j_1 = -5$). This wavelet decomposition was computed with the wavelet and the smoothing function shown in Fig. 1 and 2.

• Inverse finite wavelet transform

A finite dyadic wavelet transform is complete. We can reconstruct $f^* = S^{j_2}f \in \mathbf{V}_{j_2}$ from its finite wavelet transform

$$\mathbf{W_F}(S^{j_2}f) = \left\{ \left[W^jf(x) \right]_{j_1 \leq j < j_2} , S^{j_1}f(x) \right\} \ .$$

The inverse finite wavelet transform can also be implemented with a simple pyramidal algorithm. Let $\overline{H}(\omega)$ and $\overline{G}(\omega)$ be respectively the complex conjugate of $H(\omega)$ and $G(\omega)$. Since $|H(\omega)|^2 + |G(\omega)|^2 = 1$, equation (46) and (47) yield

$$\overline{H}(2^{-j-1}\omega)\,\hat{S}^jf(\omega) + \overline{G}(2^{-j-1}\omega)\,\hat{W}^jf(\omega) = (\,|H(2^{-j-1}\omega)|^2 + |G(2^{-j-1}\omega)|^2\,)\,\hat{S}^{j+1}f(\omega) = \hat{S}^{j+1}f(\omega) \tag{50}$$

Let $\tilde{h}^j$ and $\tilde{g}^j$ be respectively the symmetrics of h^j and g^j , the inverse Fourier transform of equation (50) can be written

$$\tilde{h}^{j+1} * S^jf(x) + \tilde{g}^{j+1} * W^jf(x) = S^{j+1}f(x) \ . \tag{51}$$

By iterating on this equation when j goes from j_1 to $j_2 - 1$, we can thus reconstruct $S^{j_2}f(x)$ from its finite

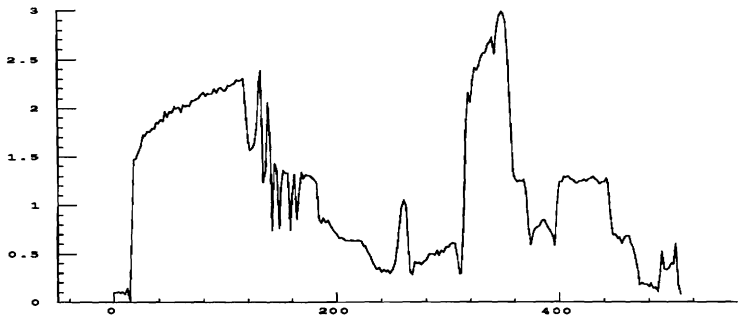

Fig. 3. *Original signal measured at the resolution* $1 : S^0 f(x)$.

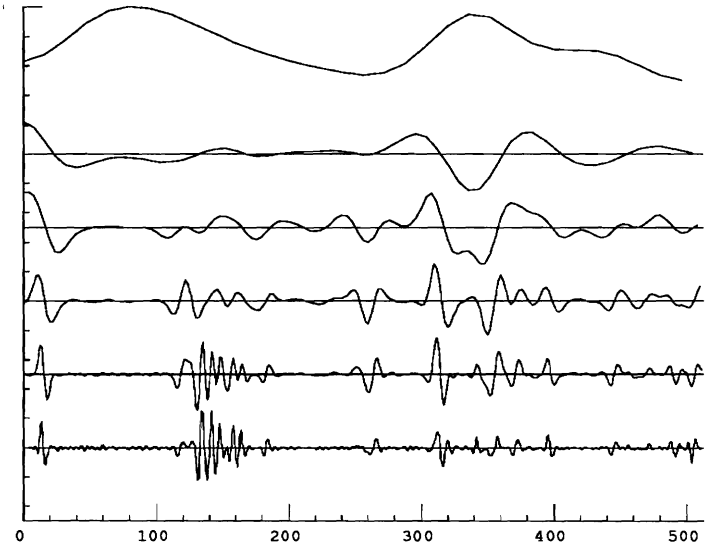

Fig. 4. *Dyadic wavelet representation of the signal shown in Fig. 3. The signal was decomposed between the scales* 1 *and* 2^{-5} *. The signal at the top is a smoothing transform of the original signal at the scale* $2^{-5} : S^{-5} f(x)$

dyadic wavelet transform. This algorithm is a characterization of the inverse finite dyadic wavelet transform $\mathbf{W_F}^{-1}$.

• Energy conservation

For a finite dyadic wavelet transform we also have a simple energy conservation property given by :

$$//S^{j_2} f(x)//^2 = \sum_{j=j_1}^{j_2-1} //W^j f(x)//^2 + //S^{j_1} f(x)//^2 \ . \tag{52}$$

This equation can easily be derived by iterating on equation (18) when j goes from j_1 to $j_2 - 1$.

• Continuity and finite wavelet transform space

Let $\mathbf{F}$ be the sub-vector space of $(\mathbf{L}^2)^{j_2-j_1}$ of the finite wavelet transform of all the functions in $\mathbf{V}_{j_2}$. The energy conservation equation shows that the operator $\mathbf{W_F}$ is an isomorphism isometric from $\mathbf{V}_{j_2}$ onto $\mathbf{F}$. The operators $\mathbf{W_F}$ and $\mathbf{W_F}^{-1}$ are thus continuous.

We are now going to characterize the vector space $\mathbf{F}$ with a projection operator from $(\mathbf{L}^2)^{j_2-j_1}$ on $\mathbf{F}$. This projector operator will also be defined from the wavelet transform $\mathbf{W_F}$ and the inverse wavelet transform $\mathbf{W_F}^{-1}$. The inverse wavelet transform $\mathbf{W_F}^{-1}$ was defined on any finite wavelet transform by iterating on equation (51). This operator can also be extended to any sequence of functions in the space $(\mathbf{L}^2)^{j_2-j_1}$. . The extension of $\mathbf{W_F}^{-1}$ will transform any sequence $\left[f_j\right]_{j_1-1\le j<j_2} \in (\mathbf{L}^2)^{j_2-j_1}$ into a function $f(x) \in \mathbf{L}^2$ with the following loop :

$$\begin{cases} \alpha_{j_1-1}(x) = f_{j_1-1}(x) \\ \text{when j goes from } j_1-1 \text{ to } j_2-1 \ : \quad \alpha_{j+1}(x) = \alpha_j * \tilde{h}^j(x) + f_j * \tilde{g}^j(x) \\ f(x) = \alpha_{j_2}(x) \end{cases}$$

As extended, the range of $\mathbf{W_F}^{-1}$ will be a sub-vector space of $\mathbf{L}^2$ which includes strictly the initial vector space $\mathbf{V}_{j_2}$. In order to be get back to the vector space $\mathbf{V}_{j_2}$ we must then apply the operator A^{j_2} which is an orthogonal projection on $\mathbf{V}_{j_2}$. Let $P_{\mathbf{F}}$ be the operator defined by

$$P_{\mathbf{F}} = \mathbf{W_F} \ o \ A^{j_2} \ o \ \mathbf{W_F}^{-1} \ . \tag{53}$$

$$(\mathbf{L}^2)^{j_2-j_1} \xrightarrow{\mathbf{W_F}^{-1}} \mathbf{L}^2 \xrightarrow{A^{j_2}} \mathbf{V}_{j_2} \xrightarrow{\mathbf{W_F}} \mathbf{F} \ .$$

This operator clearly verifies the conditions of a projection operator from $(\mathbf{L}^2)^{j_2-j_1}$ on $\mathbf{F}$:

$$\forall \left[g_j(x)\right]_{j_1-1\le j<j_2} \in (\mathbf{L}^2)^{j_2-j_1} \ , \ P_{\mathbf{F}}\left[g_j(x)\right]_{j_1\le j<j_2} \in \mathbf{F} \quad \text{and}$$

$$\left[g_j(x)\right]_{j_1-1\le j<j_2} \in \mathbf{F} \quad \text{if and only if} \quad P_{\mathbf{F}}\left[g_j(x)\right]_{j_1-1\le j<j_2} = \left[g_j(x)\right]_{j_1-1\le j<j_2} .$$

This operator expresses the intrinsic redundancy of a finite dyadic wavelet representation. It will be an important tool for analyzing any transform based on a finite dyadic wavelet representation.

The dyadic wavelet representation is a continuous representation which needs to be discretized for being used by computer algorithms. We will see in the next paragraph how one can build a complete and stable discrete wavelet transform by uniformly sampling the continuous dyadic wavelet transform.

3. Uniform sampling of infinite dyadic wavelet transforms

Ingrid Daubechies [3] has shown that it is possible to completely characterize a function f(x) by uniformly sampling the functions $W^j f(x)$ at a rate proportional to 2^j, for all scales 2^j. The functions $W^j f(x)$ are continuous because equal to the convolution of two functions in $\mathbf{L}^2$. The value of $W^j f(x)$ is thus well defined at every point. Let $r2^j$ be the sampling rate at each scale 2^j. Ingrid Daubechies has shown that any function $f(x) \in \mathbf{L}^2$ is completely characterized by the set of samples $\left[W^j f(\frac{n}{r2^j}) \right]_{(n,j)\in \mathbf{Z}^2}$. A reconstruction of the original function f(x) can be estimated from this set of samples by discretizing equation (21) :

$$f(x) = \sum_{j\in \mathbf{Z}} \sum_{n\in \mathbf{Z}} W^j f(\frac{n}{r2^j})\, \tilde{\psi}^j(x-\frac{n}{r2^j}) + \varepsilon(x) \ . \tag{54}$$

In general, for such a reconstruction, there is an error term $\varepsilon(x)$ whose energy can be estimated. An important particular case of this discrete transform has been discovered by Yves Meyer [19, 11]. Yves Meyer has shown that one could find some wavelet functions $\psi(x)$ such that $\left[\tilde{\psi}^j(x-\frac{n}{2^j}) \right]_{(n,j)\in \mathbf{Z}^2}$ is an orthonormal basis of $\mathbf{L}^2$. A wavelet orthonormal basis is a particular case of a discrete dyadic wavelet transform where $r = 1$ and $\varepsilon(x) = 0$ in equation (54). Through a multiresolution approach of these bases, it is possible to analytically characterize the Fourier transform of orthonormal wavelet functions [17]. Ingrid Daubechie has shown in particular that one could find some orthogonal wavelets which have a compact support and are n times continuously differentiable [2]. An orthogonal wavelet representation is very compact and can be used for data compression in image coding [16].

The fundamental drawback of sampled dyadic wavelet transforms for pattern recognition applications is that such representations do not translate. Let $f(x) \in \mathbf{L}^2$ and $g(x) = f(x-\tau)$, we saw in equation (20) that $W^j g(x) = W^j f(x-\tau)$. However, the sampling of $W^j g(x)$ will not correspond to a translation of the sampling of $W^j f(x)$ unless $\tau = k2^j$, $k \in \mathbf{Z}$ (see Fig. 5). A uniform sampling of a dyadic wavelet transform will thus be difficult to use in signal analysis. In the following paragraphs we will study an adaptive sampling of $W^j f(x)$ which translates when f(x) is translated. We will see that such a sampling can be defined from the zero-crossings of a dyadic wavelet representation.

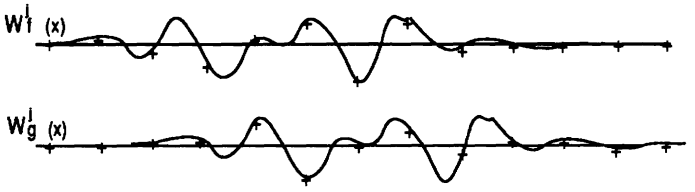

Fig. 5 *This drawing shows that the sampling of a wavelet transform (given by the crosses) is very different after translating the signal. The sampling does not translate if the translation is not proportional to the sampling rate.*

4. Energy Zero-Crossings Representation

4.1. Adaptive Sampling : Zero-Crossings

A simple adaptive sampling of the functions $\left[W^j f(x)\right]_{j\in Z}$ consists of recording the position of the zero-crossings. When f(x) is translated, $W^j f(x)$ is also translated so the position of the zero-crossings are translated as well. If $\psi(x)$ is proportional to the second derivative of a smoothing function $\theta(x)$ scaled by a factor α, any zero-crossing of $W^j f(x)$ can be interpreted as a point of abrupt change in the function f(x) smoothed by $\theta(x)$ at the scale $\alpha 2^j$. Indeed if $\psi(x) = \lambda\, \theta''(\alpha x)$,

$$W^j f(x) = f * \psi^j(x) = \lambda\ \alpha^2\, 2^{2j}\ (f(u) * \theta(\alpha 2^j u))''(x)\ . \tag{55}$$

A zero-crossing of $W^j f(x)$ will thus correspond to an inflection point of the function f(x) which had been smoothed by $\theta(x)$ at the scale $\alpha 2^j$. Fig. 6 illustrates this on a straight edge. Fig. 8 shows the wavelet decomposition of a straight edge between the scale 1 and 2^{-3}. We see that the location of the zero-crossings correspond to the location of the abrupt changes in the original signal shown in Fig. 7. In order to be proportional to the second derivative of a smoothing function, the Fourier transform $\hat{\psi}(\omega)$ of the wavelet $\psi(x)$ must verify

$$\hat{\psi}(\omega) = -\frac{\lambda}{\alpha}\, \omega^2\, \hat{\theta}\left(\frac{\omega}{\alpha}\right)\ . \tag{56}$$

Since $\theta(x)$ is a smoothing function, $\hat{\theta}(0) = 1$. The Fourier transform $\hat{\psi}(\omega)$ must therefore have a zero of order two in $\omega = 0$. The parameters α and λ are adjusted in order to have $\hat{\theta}(0) = 1$ and $//\theta// = 1$. Fig. 9 shows the smoothing function $\theta(x)$ which is proportional to the second derivative of the wavelet shown in Fig. 2.

Several researchers have studied the characterization of a function from zero-crossings properties [15, 23]. In particular, a large effort has been concentrated on the zero-crossing properties of a function convolved with the

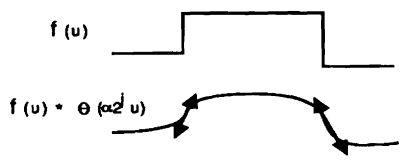

Fig. 6 *The zero-crossings of a wavelet transform provide the locations of the inflection points (edges) of* $(f(u) * \theta(\alpha 2^j u))(x)$.

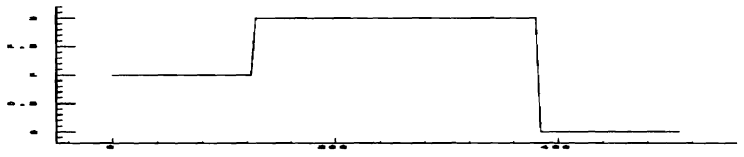

Fig. 7. *Example of straight edges.*

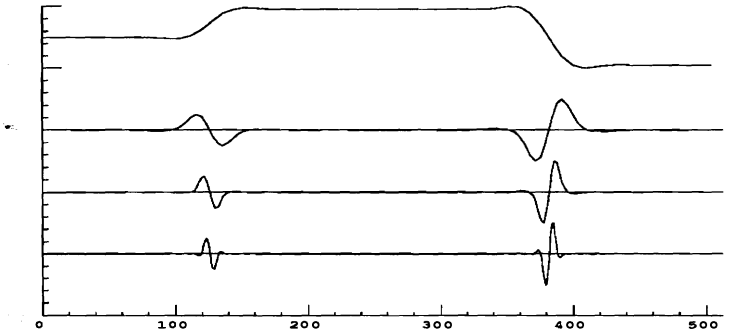

Fig. 8. *Dyadic wavelet decomposition of straight edges between the scales 1 and* 2^{-3} . *At each scale, the zero-crossings provide the location of the edges.*

Laplacian of a Gaussian [20,21,22,9]. The Laplacian of a Gaussian is not a wavelet since its Fourier transform does not verify the condition of Lemma 1. These studies are however giving some interesting preliminary results. Let us denote by $\Delta G(x)$ the Laplacian of a normalized Gaussian and $\Delta G^s(x) = \Delta G(sx)$. Bob Hummel [9] has shown that we can characterize any function $f(x) \in \mathbf{L}^2$ from the zero-crossings of $f * \Delta G^s(x)$, for all $s \in \mathbf{R}$. This characterization is however not stable. A small perturbation of the zero-crossings may correspond to an arbitrarily large distortion on the function f(x) . Bob Hummel thus proposed to stabilized the zero-crossing representation by recording the gradient along each zero-crossing. Although the derived representation seems to be stable experimentally [10], it has two disadvantages for pattern recognition applications. The convolution with a Laplacian of Gaussian corresponds to a second derivative operation on the signal, the gradient along each zero-crossing will thus correspond to a third derivative. In practice, the computation of a signal's third derivative is noisy. The

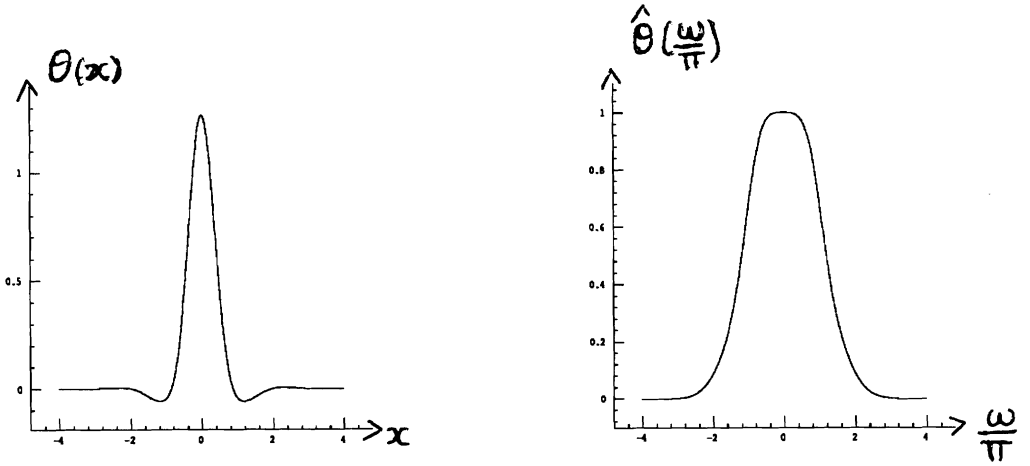

Fig. 9. *The left and right figures are respectively the graph of the smoothing function* $\theta(x)$ *and its Fourier transform* $\hat{\theta}(\frac{\omega}{\pi})$. *The second derivative of* $\theta(x)$ *is proportional to the wavelet shown in Fig. 2.*

second problem is that such a representation admits no simple metric. It is difficult to find a non ad-hoc distance which combines both the value of the gradients and the position of the zero-crossings. We thus can not easily compare two signals decomposed with such a transform. In the next paragraph we will try to stabilize the zero-crossing representation of a dyadic wavelet transform with a local energy measure. We shall see that one can then easily define a metric within such a representation. In opposition to what has been done previously with the Laplacian of Gaussian, in a dyadic wavelet transform the scale parameters vary only on a dyadic sequence $(2^j)_{j\in\mathbf{Z}}$ and not over $\mathbf{R}$ or a uniform sub-lattice of $\mathbf{R}$. We are thus keeping much less information about the zero-crossing locations.

4.2. Stabilization with local energies

Another way to stabilize a zero-crossing representation is to record the energy of $Wf(x)$ between two consecutive zero-crossings (see Fig. 10). Let (z_k^j, z_k^j) be two consecutive zero-crossings, the energy e_k^j between z_{k-1}^j and z_k^j is defined by

$$e_k^j = \left[\int_{z_{k-1}^j}^{z_k^j} |Wf(x)|^2 \, dx \right]^{1/2} \cdot sign(Wf) \; . \tag{57}$$

In the energy e_k^j we keep the sign of $Wf(x)$ on the interval $[z_{k-1}^j, z_k^j]$. This energy measures the importance of the structure which appears at the scale 2^j between the two "edges" located in z_{k-1}^j and z_k^j. The sign of the energy tells us whether the structure is convex or concave since it corresponds to the sign of a second derivative of

the signal.

We will characterize these zero-crossings and local energies with the following operator E . Let $g(x) \in \mathbf{C}$ be a continuous $\mathbf{L}^2$ functions; let $\left[z_n\right]_{n\in\mathbf{Z}}$ and $\left[e_n\right]_{n\in\mathbf{Z}}$ be respectively the positions of its zero-crossing and the values of the local energies between each pair of zero-crossings. The zero-crossings and local energies of g(x) are characterized by the piecewise constant function Eg(x) defined by :

$$\forall x \in [z_{n-1}, z_n] \quad , \quad Eg(x) = a_n = \frac{e_n}{\sqrt{z_n - z_{n-1}}} . \tag{58}$$

The function Eg(x) has the same zero-crossings as g(x) and has the same local energy between each pair of zero-crossings. We define the operator E on $\mathbf{C}$ and not over the all space $\mathbf{L}^2$ because the zero-crossings can not be defined for any function of $\mathbf{L}^2$. E is a non linear operator from $\mathbf{C}$ to the sub-vector space of $\mathbf{L}^2$ of piecewise constant functions. Since $g(x)$ and $Eg(x)$ have the same local energies, they also have the same global energy :

$$//Eg// = //g// = \sum_{n\in\mathbf{Z}} |e_n|^2 . \tag{59}$$

We shall denote by $\mathbf{E_I}$ the operator which transforms any infinite sequence of continuous functions $\left[g_j(x)\right] \in (\mathbf{C})^{\mathbf{Z}}$ into a sequence of piecewise constant functions defined by $\mathbf{E_I}\left[g_j(x)\right] = \left[Eg_j\right]$.

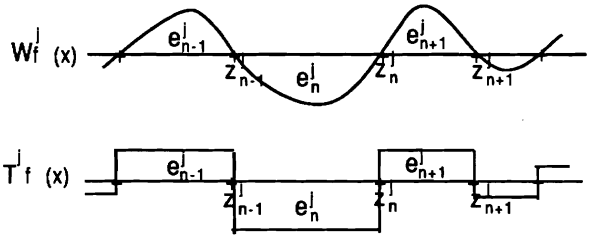

Fig. 10. *Construction of $T^j f(x)$ from $W^j f(x)$.*

At each scale 2^j, the zero-crossings and local energies of $W^j f(x)$ are characterized by the piecewise constant function $T^j f = E(Wf^j)$. Fig. 10 illustrates this transformation. We shall call **Infinite Energy Zero-Crossing** representation the set of functions

$$\mathbf{T_I} f = \left[T^j f(x)\right]_{j\in\mathbf{Z}} = \left[E(W^j f)(x)\right]_{j\in\mathbf{Z}} . \tag{60}$$

The infinite Energy Zero-Crossing representation is a sequence of piecewise constant functions which are characterized by the zero-crossings and energies of the infinite dyadic wavelet transform. The infinite Energy Zero-

Crossing transform $\mathbf{T_I}$ can be decomposed into an infinite wavelet transform $\mathbf{W_I}$ followed by the energy zero-crossing detection operator $\mathbf{E_I}$:

$$\mathbf{T_I} = \mathbf{E_I}\ o\ \mathbf{W_I}\ . \tag{61}$$

From the computer implementation point of view, at each scale 2^j , $T^j f(x)$ will be characterized by the position of its zero-crossings $\left[z_k^j\right]_{n\in\mathbf{Z}}$ and by the value of its amplitude between two zero-crossings $\left[a_k^j\right]_{n\in\mathbf{Z}}$, where

$$a_k^j = \frac{e_k^j}{\sqrt{z_k^j - z_{k-1}^j}}\ .$$

The definition of an EZC representation on a finite range of scales 2^j , for $j_1 - 1 \le j < j_2$, can similarly be derived from the definition of a finite dyadic wavelet representation. Let $S^{j_2}f \in \mathbf{V}_{j_2}$ be an approximated function at the resolution 2^{j_2} . We shall call **finite Energy Zero-Crossing** representation of $S^{j_2}f$ between the scales 2^{j_2} and 2^{j_1} , the sequence of functions

$$\mathbf{T_F}(S^{j_2}f) = \left\{ \left[T^j f(x)\right]_{j_1\le j<j_2}\ ,\ S^{j_1}f(x) \right\}\ . \tag{62}$$

Fig. 11 shows the finite EZC representation between the scales 1 and 2^{-5} of the signal shown in Fig. 3. Let $(\mathbf{C})^{j_2-j_1}$ be the set of finite sequences of continuous $\mathbf{L}^2$ functions $\left[g_j(x)\right]_{j_1-1\le j<j_2}$. Let $\mathbf{E_F}$ denote the operator which transforms any sequence of function $\left[g_j(x)\right]_{j_1-1\le j<j_2} \in (\mathbf{C})^{j_2-j_1}$ into the sequence of functions $\left\{ \left[Eg_j(x)\right]_{j_1\le j<j_2}, g_{j_1-1}(x) \right\}$. The finite EZC transform operator $\mathbf{T_F}$ can be decomposed into a finite wavelet transform followed by the operator $\mathbf{E_F}$:

$$\mathbf{T_F} = \mathbf{E_F}\ o\ \mathbf{W_F}\ .$$

5. Properties of an Energy Zero-Crossings representation

• Translating property

An Energy Zero-Crossings representation is clearly translating when the signal translates. Indeed, the zero-crossings of $W^j f(x)$ are translated and the energies between two zero-crossings are not modified.

$$\text{If}\quad g(x) = f(x-\tau)\ ,\ \forall j \in \mathbf{Z}\quad ,\quad T^j g(x) = T^j f(x-\tau)\ . \tag{63}$$

• Energy conservation

We can derive an energy conservation property from equation (59) and from the energy conservation equations of

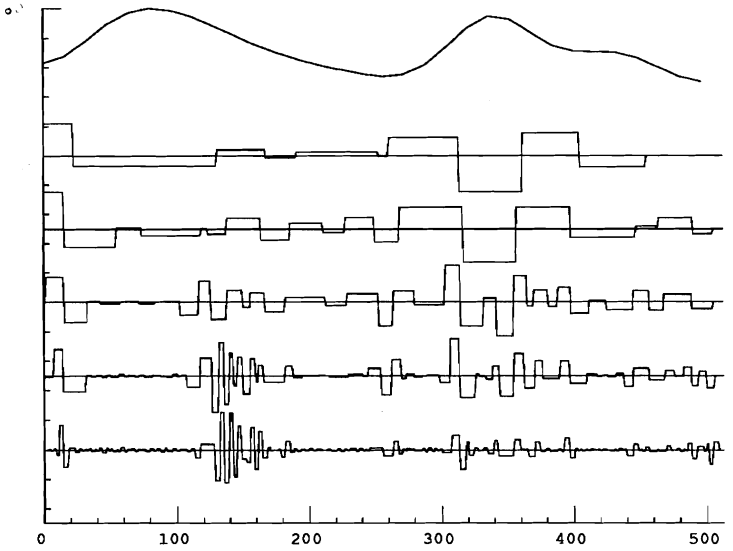

Fig. 11. *Energy Zero-Crossing representation of the signal shown in Fig. 3. It is derived from the zero-crossings and local energies of the wavelet transform shown in Fig. 4. The top curve is* $S^{-5}f(x)$ *and the other piecewise constant curves are the graphs of* $T^j f(x)$ *for* $0 > j \geq -5$.

a dyadic wavelet transform.

For an infinite energy zero-crossing representation we have :

$$\forall f(x) \in \mathbf{L}^2 \quad , \quad \|f\|^2 = \sum_{j \in \mathbf{Z}} \|T^j f\|^2 \ . \tag{64}$$

In the case of a finite energy zero-crossing representation the energy conservation is expressed by :

$$\forall S^{j_2} f \in \mathbf{V}_{j_2} \quad , \quad \|S^{j_2} f(x)\|^2 = \sum_{j=j_1}^{j_2} \|T^j f\|^2 + \|S^{j_1} f(x)\|^2 \ . \tag{65}$$

5.1. Distance on the Energy Zero-Crossing representation

A natural distance on the EZC representations can be derived from the energy conservation equations (64) and (65). For an infinite EZC representation, this distance is defined as follow. Let $f(x) \in \mathbf{L}^2$, $g(x) \in \mathbf{L}^2$ and $\mathrm{T_I}f$, $\mathrm{T_I}g$ be respectively their EZC representation,

$$\mathbf{d}(\mathrm{T_I}f \ , \mathrm{T_I}g \ ) = \left[\sum_{j \in \mathbf{Z}} \|T^j f - T^j g\|^2 \right]^{1/2} \ . \tag{66}$$

One can easily verify that **d** is indeed a distance. The energy conservation equations can be written

$$\mathbf{d}(\mathrm{T_I}f \ , 0 \ ) = \|f\| \ . \tag{67}$$

For any pair of functions f(x) and g(x) in $\mathbf{L}^2$ we also have

$$\mathbf{d}(\mathbf{T}_I f , \mathbf{T} g) \leq \mathbf{d}(\mathbf{T}_I f , 0) + \mathbf{d}(\mathbf{T}_I g , 0) = //f// + //g// \ .$$

The distance $\mathbf{d}$ is thus closely related to the norm in $\mathbf{L}^2$. In the finite case the distance $\mathbf{d}$ is similarly defined. Let $S^{j_2} f(x) \in \mathbf{V}_{j_2}$ and $S^{j_2} g \in \mathbf{V}_{j_2}$ be two functions approximated at the resolution 2^{j_2}. The distance between the two corresponding finite EZC representations is defined by

$$\mathbf{d}(\mathbf{T}_F(S^{j_2} f) , \mathbf{T}_F(S^{j_2} g)) = \left[\sum_{j=j_1}^{j_2-1} //T^j f - T^j g//^2 + //S^{j_1} f - S^{j_1} g//^2 \right]^{1/2} \ . \tag{68}$$

We can also derive from the energy conservation equation (65) that

$$\mathbf{d}(\mathbf{T}_F(S^{j_2} f) , 0) = //S^{j_2} f // \quad \text{and} \tag{69}$$

$$\mathbf{d}(\mathbf{T}_F(S^{j_2} f) , \mathbf{T}_F(S^{j_2} g)) \leq //S^{j_2} f // + //S^{j_2} g // \ . \tag{70}$$

Since $T^j f(x)$ and $T^j g(x)$ are piecewise constant functions, the integral

$$//T^j f - T^j g//^2 = \int_{-\infty}^{+\infty} (T^j f(x) - T^j g(x))^2 \, dx \tag{39}$$

is simple and quick to compute. It is calculated by multiplying the amplitude values of $T^j f(x)$ and $T^j g(x)$ between each pair of zero-crossings. The distance $\mathbf{d}$ can thus be easily implemented.

The distance $\mathbf{d}$ as previously defined is a global distance which compares two EZC representations over the entire spatial domain. A pattern is often a local feature embedded in the signal. For pattern matching purposes, we need to define a local distance which compares locally two EZC representations. In order to derive such a distance from $\mathbf{d}$, we will study the decomposition at all scales of a local feature such as a dirac $\delta_{x_0}(x)$ centered in x_0.

$$W^j \delta_{x_0}(x) = \delta_{x_0} * \psi^j(x) = \psi^j(x - x_0) \ . \tag{71}$$

Let σ be the size of the interval on which the energy of $\psi(x)$ is mostly concentrated :

$$\int_{-\sigma}^{\sigma} \psi^2(x) \, dx \approx \int_{-\infty}^{+\infty} \psi^2(x) \, dx \ . \tag{72}$$

Equations (71) and (72) show that the energy of $W^j \delta_{x_0}(x)$ is mainly concentrated on the interval $[x_0 - 2^{-j}\sigma , x_0 + 2^{-j}\sigma]$. This implies that

$$T^j \delta_{x_0}(x) \approx 0 \quad \text{for} \quad |x - x_0| \geq 2^{-j} \sigma \ . \tag{72}$$

In the case of an infinite EZC representation, it is thus natural to define the following local distance $\mathbf{d}_{x_0}$ for

comparing two representations in the neighborhood of a point x_0 :

$$\mathbf{d}_{x_0}(\mathbf{T}_I f\ ,\mathbf{T}_I g\ ) = \left[\sum_{j\in\mathbf{Z}} \int_{x_0-2^{-j}\sigma}^{x_0+2^{-j}\sigma} (T^j f(x) - T^j g(x))^2\, dx \right]^{1/2}. \tag{73}$$

For a finite EZC representation, the local distance $\mathbf{d}_{x_0}$ is given by

$$\mathbf{d}_{x_0}(\mathbf{T}_F(Sj2f)\ ,\mathbf{T}_F(Sj2g)) = \left[\sum_{j\in\mathbf{Z}} \int_{x_0-2^{-j}\sigma}^{x_0+2^{-j}\sigma} (T^j f(x) - T^j g(x))^2\, dx \ + \int_{x_0-2^{-j}\sigma}^{x_0+2^{-j}\sigma} (S^{j_1} f(x) - S^{j_1} g(x))^2\, dx \right]^{1/2} \tag{74}$$

When matching patterns with a coarse to fine strategy, we will decompose the local distance $\mathbf{d}_{x_0}$ into a sum of local distances $\mathbf{d}_{x_0}^j$ such that

$$\mathbf{d}_{x_0}^j(T^j f\ ,T^j g\ ) = \left[\int_{x_0-2^{-j}\sigma}^{x_0+2^{-j}\sigma} (T^j f(x) - T^j g(x))^2\, dx \right]^{1/2}. \tag{75}$$

$\mathbf{d}_{x_0}^j(T^j f\ ,T^j g)$ is a measure of the local distortion between f(x) and g(x) around the point x_0, at the scale 2^j.

5.2. Completeness of the Energy Zero-Crossing representation

In this paragraph we will study the completeness of the finite Energy Zero-Crossing representation. The finite Energy Zero-Crossing representation is complete if and only if the operator $\mathbf{T}_F$ admits an inverse $\mathbf{T}_F^{-1}$ on its range. Since $\mathbf{T}_F = \mathbf{E}_F\, o\, \mathbf{W}_F$ and $\mathbf{W}_F$ is an isomorphism of $\mathbf{V}_{j_2}$ onto $\mathbf{F}$, we must prove that the restriction of the operator $\mathbf{E}_F$ to the vector space $\mathbf{F}$ is invertible on its range. This problem is difficult to solve mathematically because $\mathbf{E}_F$ is a non linear operator. We will thus take an experimental approach to and show that one can develop an iterative algorithm which implements the inverse of the restriction of $\mathbf{E}_F$ to $\mathbf{F}$.

For any function $S^{j_2}f \in \mathbf{V}_{j_2}$, we want to reconstruct the finite wavelet transform $\mathbf{W}_F(S^{j_2}f)$ from the EZC representation $\mathbf{T}_F(S^{j_2}f)$. We must therefore characterize each function $W^j f(x)$ with the positions of its zero-crossings and the values of its local energies. Let $\Gamma\mathbf{f}$ be the set of all the sequences $\left[g_j(x)\right]_{j_1-1\le j<j_2} \in (\mathbf{C})^{j_2-j_1}$, such that $\mathbf{E}_F\left[g_j(x)\right]_{j_1\le j<j_2} = \mathbf{T}_F(S^{j_2}f)$. For any such sequence, $g_{j_1-1}(x) = S^{j_1}f(x)$ and for all integers $j_1 \le j < j_2$, the zero-crossings and local energies of $g_j(x)$ and $T^j f(x)$ are the same. $\Gamma\mathbf{f}$ is clearly not a vector space. The wavelet representation $\mathbf{W}_F(S^{j_2}f)$ is a member of the intersection of $\Gamma\mathbf{f}$ and $\mathbf{F}$. If the restriction of $\mathbf{E}_F$ to $\mathbf{F}$ is injective than this intersection is reduced to $\mathbf{W}_F f$:

$$\Gamma\mathbf{f} \cap \mathbf{F} = \left\{ \mathbf{W}_F(S^{j_2}f) \right\}. \tag{76}$$

We have defined in (53) a linear projection operator P_F on the vector space $\mathbf{F}$. Let $P_{\Gamma\mathbf{f}}$ be a projector on $\Gamma\mathbf{f}$.

Since Γf is not a vector space $P_{\Gamma f}$ is a non linear operator. By definition $P_{\Gamma f}$ verifies the following two properties :

$$\forall \left[g_j \right]_{j_1-1 \le j < j_2} \in (\mathbf{C})^{j_2-j_1} \ , \quad P_{\Gamma f}\left[g_j \right]_{j_1-1 \le j < j_2} \in \Gamma f \quad \text{and} , \tag{77}$$

$$\left[g_j \right]_{j_1-1 \le j < j_2} \in \Gamma f \quad \text{if and only if} \quad P_{\Gamma f}\left[g_j \right]_{j_1-1 \le j < j_2} = \left[g_j \right]_{j_1-1 \le j < j_2} . \tag{78}$$

Since the wavelet transform $\mathbf{W}_F(S^{j_2}f)$ is a member of the intersection of Γf and $\mathbf{F}$, it is a fixed point of both operators $P_{\Gamma f}$ and P_F. If the EZC representation is complete then assertion (76) shows that $\mathbf{W}_F(S^{j_2}f)$ is the unique common fixed point of these two operators. Let $\mathbf{O}$ be a composition of $P_{\Gamma f}$ with P_F

$$\mathbf{O} = P_F \, o \, P_{\Gamma f} \ . \tag{79}$$

$\mathbf{W}_F(S^{j_2}f)$ is also a fixed point of $\mathbf{O}$. We are going to use this property to reconstruct $\mathbf{W}_F(S^{j_2}f)$ from the EZC representation $\mathbf{T}_F(S^{j_2}f)$.

A classical method for computing a fixed point is to iterate on the operator from a given initial point. Let $\mathbf{O}^n$ be the composition n times of the operator $\mathbf{O}$ and I be an initial point in $(\mathbf{C})^{j_2-j_1}$. We would like to show that

$$\lim_{n \to \infty} \mathbf{O}^n(I) = \mathbf{W}_F(S^{j_2}f) \ . \tag{80}$$

Fig. 12 illustrates the principle of this reconstruction algorithm.

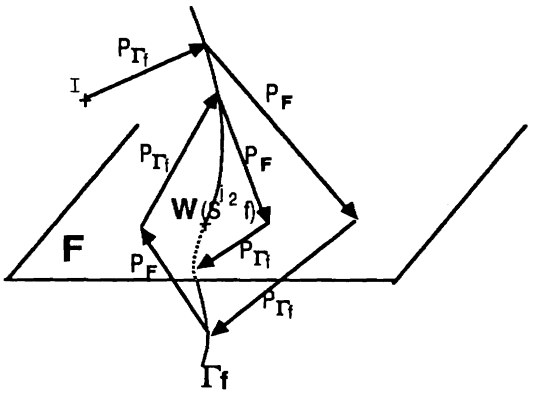

Fig. 12 *Illustration of the reconstruction algorithm.* Γf *is symbolized by a curve and* $\mathbf{F}$ *by a plane. By iterating on a composition of the operators* $P_{\Gamma f}$ *and* P_F, *we want to reach* $\mathbf{W}_F(S^{j_2}f)$ *which is at the intersection of* Γf *and* $\mathbf{F}$. *The intial point I is anywhere in* $(\mathbf{C})^{j_2-j_1}$.

Since the operator $\mathbf{O}$ is not a contracting operator, the algorithm might not converge from any initial point. With the implementation of the operator $\mathbf{O}$ described in paragraph 6.2, we have shown experimentally that for any initial point I the algorithm does converge. In about ten iterations, the function $\mathbf{O}^n(I)$ gives a very good reconstruction of $\mathbf{W_F}(S^{j_2}f)$. Fig. 13 shows the result of such an iteration by using the EZC representation given in Fig. 11. The quality of the reconstruction can be appreciated by comparing this reconstruction with the original wavelet decomposition shown in Fig. 4. From the reconstruction of this wavelet transform, we have reconstructed the original signal by applying the inverse wavelet transform operator $\mathbf{W_F}^{-1}$. The reconstruction of the approximated function is shown in Fig. 14. We have obtained the same quality of reconstruction for all the signal that we have decomposed. The signal shown in Fig.3 is the scan line of an image. We have also tested the reconstruction algorithm on some particularly interesting functions of $\mathbf{V}_{j_2}$. We have shown numerically that if $S^{j_2}f = \rho^{j_2}(x)$ or $S^{j_2}f = \xi^{j_2}(x)$ the reconstruction algorithm also converges towards the original wavelet representation. By applying the inverse wavelet transform operator $\mathbf{W_F}^{-1}$, we have then been able to reconstruct the original functions $\rho^{j_2}(x)$ and $\xi^{j_2}(x)$. Since the representation is translating, this shows that we can reconstruct any function of the two families $\left(\rho^{j_2}(x-2^{-j_2}n)\right)_{n\in\mathbf{Z}}$ and $\left(\xi^{j_2}(x-2^{-j_2}n)\right)_{n\in\mathbf{Z}}$. As shown in paragraph 2.3.1, each of these families is a basis of the vector space $\mathbf{V}_{j_2}$. However, since the operator $\mathbf{T_F}$ is not linear, this does not enable us to conclude anything about the reconstruction of any function $S^{j_2}f \in \mathbf{V}_{j_2}$. For all the signals that we have tested, five iterations are enough for having a good reconstruction of the finite dyadic wavelet transform. At the highest scales 2^j, it takes a few more iterations for reconstructing properly the wavelet transforms $Wjf(x)$. When we decrease the value of j_1, the quality of the reconstruction is not modified.

A Wavelet transform and thus an Energy Zero-Crossing representation is defined with respect to a wavelet function $\psi(x)$. The examples shown in this paper were computed with the wavelet $\psi(x)$ shown in Fig. 2. We have also tested the reconstruction with another wavelet which was much less regular. This other wavelet was derivable but not continuously derivable. Very similar results were obtained on the EZC representation defined with respect to this other wavelet.

This reconstruction algorithm cannot provide a proof for the completeness of a finite Energy Zero-Crossing representation since we cannot make an extensive test on all the possible signals $S^{j_2}f \in \mathbf{V}_{j_2}$. However, given these reconstructions, it is likely that the representation is indeed complete for any kind of signal in $\mathbf{V}_{j_2}$ or at least for a very large class of functions within this vector space.

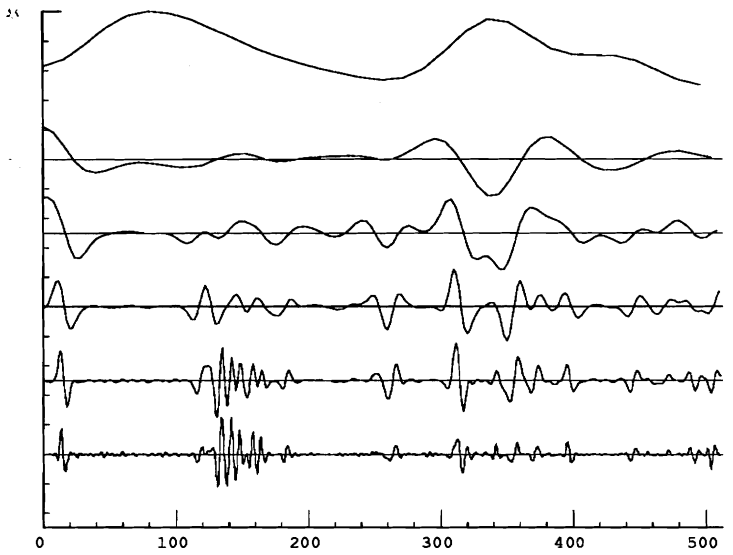

Fig. 13 *Reconstruction of the dyadic Wavelet transform with the iterative algorithm previously described. The quality of this reconstruction can be appreciated by comparing this graph with the original wavelet transform shown in Fig. 4.*

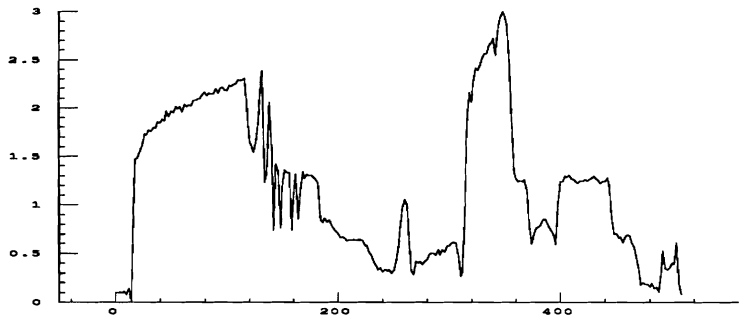

Fig. 14 *Reconstruction of the original signal by applying the inverse wavelet transform operator on the wavelet reconstruction shown in Fig. 13. The quality of this reconstruction can be appreciated by comparing this graph with the original signal shown in Fig. 3.*

5.3. Continuity

We will see in this paragraph that the operators $\mathbf{T_F}$ and $\mathbf{T_I}$ can have some local discontinuities when some zero-crossings are created or disappear at a scale 2^j . We will study this problem for a finite EZC representation but the same result will apply for an infinite representation. The operator $\mathbf{T_F}$ is said to be continuous if for any signal $S^{j_2}f \in \mathbf{V}_{j_2}$ the addition of a signal $\varepsilon(x)$ of small energy produces only a small distortion on the EZC

representation of $S^{j_2}f(x)$. This continuity cannot be derived from the energy conservation equation because $\mathbf{T_F}$ is not a linear operator. Since $\mathbf{T_F} = \mathbf{E_F}\, o\, \mathbf{W_F}$ and since we know that $\mathbf{W_F}$ is continuous, the continuity of $\mathbf{T_F}$ depends on the continuity of the restriction of $\mathbf{E_F}$ to $\mathbf{F}$. The continuity of the restriction of $\mathbf{E_F}$ would mean that if $//\mathbf{W_F}(f) - \mathbf{W_F}(f+\varepsilon)//$ is small then $\mathbf{d}(\mathbf{T_F}(S^{j_2}f), \mathbf{T_F}(S^{j_2}(f+\varepsilon)))$ remains small. We our going to show that this is not true if the perturbation $\varepsilon(x)$ creates or suppresses a pair of zero-crossings in $W^j f(x)$ at a given scale 2^j. This discontinuity phenomenon is illustrated by Fig. 15.

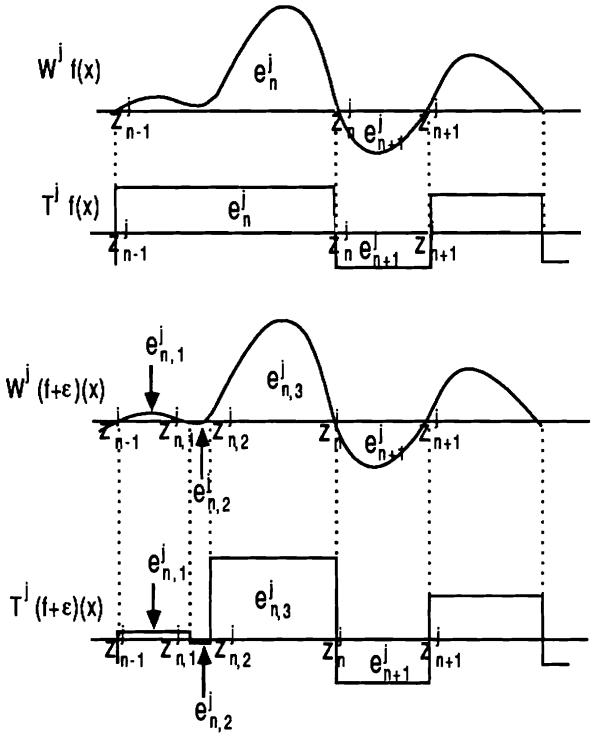

Fig. 15 *When creating a new zero-crossing, a small perturbation* $\varepsilon(x)$ *can significantly modify the Energy Zero-Crossing representation. The energy* e_k^j *is suddenly divided into* $e_{1,n}^j$, $e_{2,n}^j$ *and* $e_{3,n}^j$.

Let $(z_{k,1}^j , z_{k,2}^j)$ be a pair of zero-crossings created by the perturbation $\varepsilon(x)$ between two zero-crossings (z_{k-1}^j , z_k^j) of $W^j f(x)$. The energy e_k^j of $W^j f(x)$ in the interval $[z_{k-1}^j , z_k^j]$ is suddenly divided into $e_{k,1}^j$, $e_{k,2}^j$ and $e_{k,3}^j$. If the perturbation $\varepsilon(x)$ is small then $e_{k,1}^j + e_{k,3}^j \approx e_k^j$, $e_{k,2}^j \approx 0$ and $z_{k,1}^j = z_{k,2}^j$. Even if the perturbation $\varepsilon(x)$ has a very low energy, $T^j(f+\varepsilon)$ can be significantly different from $T^j f$ between the zero-crossings z_{k-1}^j and z_k^j (see Fig. 15). Equation (81) gives an estimation of the distortion due to the apparition of a new pair of zero-crossings :

$$\int_{z_{k-1}^j}^{z_k^j} (T^j f(x) - T^j(f+\varepsilon)(x))^2\, dx \;\le\; \left(e_k^j \sqrt{\frac{z_{k,1}^j - z_{k-1}^j}{z_k^j - z_{k-1}^j}} - e_{k,1}^j \right)^2 + \left(e_k^j \sqrt{\frac{z_k^j - z_{k,2}^j}{z_k^j - z_{k-1}^j}} - e_{k,3}^j \right)^2 . \qquad (81)$$

In general a small perturbation will create or suppress pairs of zero-crossings in regions of low local energies. The perturbation estimated by equation (81) will then be small. It is also important to observe that the distortion of $T_F(S^{j_2}f)$ introduced by new zero-crossings remains localized. The overall representation $T_F(S^{j_2}f)$ is not modified. When testing the EZC representation on the stereo-matching problem, we will see that these local discontinuities do not disturb much the matching process.

We saw in the previous paragraph that the operator T_F is likely to be invertible on its range. Let us suppose that it is indeed invertible and let us denote by T_F^{-1} its inverse. The inverse operator T_F^{-1} is said to be continuous if any small perturbation of a representation $T_F f$ measured with $\mathbf{d}$ corresponds to a small distortion of the original signal f(x) . Since the inverse wavelet operator W_F^{-1} is continuous, it is sufficient to prove that the wavelet transform $W_F f$ is only slightly modified. In this case we do not have any problem related to the creation of new pairs of zero-crossings since the EZC representation is supposed to be only slightly perturbated. The fact that our reconstruction algorithm does converge shows experimentally that any small perturbation of $T_F f$ corresponds to a small distortion of the associated wavelet representation $W_F f$. As we said in the previous paragraph, this not a proof since we cannot test the algorithm on all the functions $S^{j_2}f \in \mathbf{V}_{j_2}$.

6. Numerical algorithms

In this paragraph we will describe the numerical implementation of a finite Energy Zero-Crossing transform. We will then show how to compute the reconstruction algorithm described in paragraph 5.2 .

6.1. Implementation of a finite EZC representation

In the following, we are going to detail the computation of a finite EZC representation for any signal approximated at a resolution 1 . We will suppose that our measuring device provides us with a uniform sampling at the rate 1 of a signal approximated at the resolution 1 . Theorem 2 shows how to interpolate between these samples for computing the value of this approximated signal everywhere. In order to calculate an EZC representation, we must first compute the corresponding dyadic wavelet representation. We will estimate the position of the zero-crossings and the value of the local energies of this wavelet transform. In practice we cannot compute the values of the functions $W^j f(x)$ at every point. We can only calculate a uniform sampling of these functions. In order to estimate the positions of the zeros and the value of the energies with a similar precision for all the scales 2^j , we must sample $W^j f(x)$ at a rate proportional to 2^j . In order to simplify the implementation we will choose a sampling rate which is a power of 2 . Let 2^{j_0+j} be the sampling rate at each scale 2^j . We will show that we can develop a discrete pyramidal algorithm for computing a uniform sampling of each function $W^j f(x)$ at the rate 2^{j_0+j} . The position of the zero-crossings and the values of the local energies will then be estimated with a simple

linear interpolation between the samples of the functions $W^j f(x)$.

6.1.1. Dyadic wavelets for discrete algorithms

We are going to define in this paragraph a particular sub-class of dyadic wavelets which will enable us to compute a discrete wavelet transform with a pyramidal algorithm. We saw in paragraph 2.1 that any smoothing function $\phi(x)$ has a Fourier transform $\hat{\phi}(\omega)$ which can then be written

$$\hat{\phi}(\omega) = \prod_{p=1}^{+\infty} H(2^{-p}\omega) \quad . \tag{82}$$

The Fourier transform of an associated wavelet $\psi(x)$ can be expressed as

$$\hat{\psi}(\omega) = G(\frac{\omega}{2})\,\hat{\phi}(\frac{\omega}{2}) \quad \text{where} \quad |G(\omega)|^2 + |H(\omega)|^2 = 1 \quad . \tag{83}$$

As explained in paragraph 4.1, we are interested in wavelets $\psi(x)$ which are proportional to the second derivative of a smoothing function $\theta(x)$. We saw in equation (56) that the Fourier transform $\hat{\psi}(\omega)$ must then have a zero of order two in $\omega = 0$. Equation (83) implies that $G(\omega)$ must also have a zero of order two in zero. This will be verified if and only if the first three derivatives of $H(\omega)$ are equal to zero in $\omega = 0$. To be able to compute a discrete wavelet transform with a pyramidal algorithm, we will also suppose that $H(\omega)$ and $G(\omega)$ are $2\pi 2^{j_\sigma - 1}$ periodic. The functions $H(\omega)$ and $G(\omega)$ can then be written as Fourier series :

$$H(\omega) = \sum_{n \in \mathbf{Z}} h_n \, e^{in 2^{j_\sigma - 1}\omega} \quad \text{and} \quad G(\omega) = \sum_{n \in \mathbf{Z}} g_n \, e^{in 2^{j_\sigma - 1}\omega} \quad . \tag{84}$$

The inverse Fourier transforms of $H(\omega)$ and $G(\omega)$ as defined in paragraph 2.3.2 are respectively the distributions given by :

$$h(x) = \sum_{n \in \mathbf{Z}} h_n \, \delta(x - n 2^{j_\sigma - 1}) \quad \text{and} \quad g(x) = \sum_{n \in \mathbf{Z}} g_n \, \delta(x - n 2^{j_\sigma - 1}) \quad .$$

We will represent these two distributions by the two $\mathbf{l}^2(\mathbf{Z})$ sequences $h = \left[h_n \right]_{n \in \mathbf{Z}}$, $g = \left[g_n \right]_{n \in \mathbf{Z}}$ and call them discrete filters. In the next paragraph we will see that we can compute a discrete wavelet decomposition by convolving successively the signal with these two discrete filters.

We are now going to describe the particular wavelet transform which has been used for computing the examples shown in this paper. In this particular case we chose a sampling coefficient 2^{j_0} equal to 8 ($j_0 = 3$). The Fourier transform of the smoothing function shown in Fig. 1 corresponds to a function $H(\omega)$ which is 8π periodic and such that

$$H(\omega) = e^{-\frac{\omega^4}{19.25}} \quad \text{for } \omega \in [-4\pi, 4\pi] \quad . \tag{85}$$

The coefficient 19.25 was adjusted numerically in order to have $//\phi// = 1$. We do not have any general characterization of the functions $H(\omega)$ which would enable us adjust the norm of $\phi(x)$. The Fourier transform of the associated wavelet shown in Fig. 2 corresponds to $G(\omega) = -\sqrt{1 - H(\omega)^2}$. Fig. 16 gives the corresponding values of the two discrete filters $h = \left[h_n\right]_{n\in\mathbf{Z}}$ and $g = \left[g_n\right]_{n\in\mathbf{Z}}$.

n	h_n	g_n	n	h_n	g_n
0	0.151	-0.898	8	-0.014	0.012
1	0.144	0.100	9	-0.015	0.004
2	0.125	0.092	10	-0.013	-0.001
3	0.097	0.080	11	-0.008	-0.003
4	0.066	0.066	12	-0.003	-0.004
5	0.035	0.050	13	0.000	-0.003
6	0.011	0.035	14	0.002	-0.002
7	-0.006	0.022	15	0.002	-0.001

Fig. 16 *Coefficients of the discrete filters* h, g. *These filters are symmetrical :* $h_{-n} = h_n$ and $g_{-n} = g_n$.

6.1.2. Interpolation of a finite resolution approximation

In this paragraph, we will describe the interpolation of a discrete approximated signal and explain how to compute a scaling function to define the concept of resolution. Let us suppose that our measuring device provides us with a uniform sampling at the rate 1 of a signal measured at the resolution 1. Let $S^0f(x) \in \mathbf{V}_0$ denote this approximated signal; the uniform sampling corresponds to $\left[S^0f(n)\right]_{n\in\mathbf{Z}}$. As we shall see in paragraph 6.1.3, in order to apply the discrete pyramidal algorithm which computes the discrete wavelet transform of S^0f, we must first calculate a uniform sampling of $S^0f(x)$ at a rate 2^{j_0-1}. Such a sampling can be calculated with the spline function $\rho(x)$ defined in theorem 3. Indeed, we saw in theorem 3 that

$$S^0f(x) = \sum_{k=-\infty}^{+\infty} S^0f(k)\,\rho(x-k) \quad .$$

For any sample $n2^{-j_0+1}$ we have

$$S^0f(n2^{-j_0+1}) = \sum_{k=-\infty}^{+\infty} S^0f(k)\,\rho(n2^{-j_0+1}-k) \quad . \tag{86}$$

This equation shows that the interpolated discrete signal $S^0 f(n2^{-j_0+1})$ can be computed by putting $2^{j_0-1}-1$ zeros in between each sample of $\left[S^0 f(n)\right]_{n\in Z}$ and convolving the resulting signal with the discrete interpolation filter $\rho_d = \left[\rho(n2^{-j_0+1})\right]_{n\in Z}$.

Let us now discuss the choice of a scaling function to implement the concept of resolution. Theorem 2 shows that the Fourier transform $\hat{\xi}(\omega)$ of a scaling function can be computed from a function $X(\omega)$ satisfying the properties (a) , (b) and (c) . In order to be able to define a finite dyadic wavelet transform, the scaling function $\xi(x)$ must also verify the conditions of lemma 2. The Fourier transform $\hat{\xi}(\omega)$ must have a decay at infinity which is faster than $\frac{\hat{\phi}(\omega)}{\omega}$:

$$\hat{\xi}(\omega) = O(\frac{\hat{\phi}(\omega)}{\omega}) \quad \text{at infinity} .$$

This condition will always be verified if the Fourier transform of $\xi(x)$ has a compact support. The scaling functions whose Fourier transform have a compact support have been studied by Yves Meyer [19]. They correspond to a function $X(\omega)$ equal to 1 on the interval $[-\frac{\pi}{3}, \frac{\pi}{3}]$. The inconvenience of these scaling functions is that they have a slow effective decay at infinity in the spatial domain. The interpolation function $\rho(x)$ defined in theorem 3 will also have a slow decay. This means that the coefficients of the interpolation filter ρ_d will decrease slowly. It is then more efficient to compute the convolution product of the interpolation (86) with a multiplication in the Fourier domain.

If we want to be able to compute directly the interpolation equation in the spatial domain, we must choose a scaling function $\xi(x)$ which has a faster effective decay at infinity. This function was studied by P. Y. Lemarie [13]. In each interval $[k, k+1]$ the function $\xi(x)$ is a polynomial of order three. Its Fourier transform is given by

$$X(\omega) = \sqrt{\frac{\Sigma_8(\omega)}{2^8 \Sigma_8(2\omega)}} \quad \text{and} \quad \hat{\xi}(\omega) = \frac{1}{\omega^4 \sqrt{\Sigma_8(\omega)}} \quad \text{where} \tag{87}$$

$$\Sigma_8(\omega) = \sum_{-\infty}^{+\infty} \frac{1}{(\omega+2k\pi)^8} .$$

The function $\Sigma_8(\omega)$ can be computed with the following formula

$$\Sigma_8(\omega) = \frac{105\,(sin\frac{\omega}{2})^8}{\pi^8\,(\,5+30\,(cos\frac{\omega}{2})^2+30\,(sin\frac{\omega}{2})^2\,(cos\frac{\omega}{2})^2+2\,(sin\frac{\omega}{2})^4\,(cos\frac{\omega}{2})^2+70\,(cos\frac{\omega}{2})^4+\frac{2}{3}\,(sin\frac{\omega}{2})^6\,)} .$$

With theorem 3 we can derive that the Fourier transform of the spline function is equal to

$$\hat{\rho}(\omega) = \left[\frac{\sin\frac{\omega}{2}}{\frac{\omega}{2}}\right]^4 (1-\frac{2}{3}\sin^2\frac{\omega}{2})^{-1} . \tag{88}$$

In this particular case, the function $\rho(x)$ is cubic spline polynomial. The coefficients of the filter ρ_d are given in Fig. 17 for $j_0 = 3$.

n	$\rho(\frac{n}{4})$	n	$\rho(\frac{n}{4})$	n	$\rho(\frac{n}{4})$	n	$\rho(\frac{n}{4})$
0	1	4	0	8	0	12	0
1	0.881	5	-0.123	9	0.033	13	-0.008
2	0.600	6	-0.127	10	0.034	14	-0.009
3	0.269	7	-0.068	11	0.018	15	-0.005

Fig. 17 *Coefficients of the discrete filter* $\left[\rho(n2^{-j_0+1})\right]_{n\in\mathbf{Z}}$ *for* $j_0 = 3$. *This filter is symmetrical.*

6.1.3. Discrete wavelet transform pyramidal algorithm

In this paragraph, we are going to describe the pyramidal implementation of a discrete wavelet transform. This algorithm is a generalization of an algorithm that we developed [16] for orthogonal wavelets. It can also be viewed as a discretization of the pyramidal algorithm described in paragraph 2.3.2 for computing a finite dyadic wavelet transform. Let $S^0 f(x) \in \mathbf{V}_0$ be the approximated signal that we want to decompose. Let $W^j f_d$ denote the discrete signal equal to a uniform sampling of $W^j f(x)$ at a rate 2^{j_0+j} :

$$W^j f_d = \left[W^j f(k2^{-j_0-j})\right]_{k\in\mathbf{Z}} = \left[f * \psi^j(k2^{-j_0-j})\right]_{k\in\mathbf{Z}} . \tag{89}$$

Let us also denote by $S^j f_d$ the discrete signal equal to a uniform sampling of $S^j f(x)$ at a rate 2^{j_0+j-1} :

$$S^j f_d = \left[S^j f(k2^{-j_0-j+1})\right]_{k\in\mathbf{Z}} = \left[f * \phi^j(k2^{-j_0-j+1})\right]_{k\in\mathbf{Z}} . \tag{90}$$

Let 2^{-J} the minimum resolution where we want to stop our wavelet decomposition. We are going to explain the computation of the discrete wavelet transform $\left\{\left[W^j f_d\right]_{0>j\geq -J}, S^{-J} f_d\right\}$.

As described in paragraph 6.1.2, we will suppose that we have been able to compute a uniform sampling at the rate 2^{j_0-1} of the approximated signal $S^0 f(x)$ that we want to decompose. This uniform sampling corresponds to the discrete signal $S^0 f_d$. The following Lemma shows that for any scale 2^j , one can decompose $S^{j+1} f_d$ into $S^j f_d$ and $W^j f_d$ by convolving this discrete signal with the two filters h and g . This Lemma is a discrete equivalent of equations (48) and (49).

Lemma 3

$$\forall j \in \mathbf{Z} \quad , \quad W^j f_d = S^{j+1} f_d * g \quad \text{and} \tag{91}$$

$$\text{if} \quad \left[\lambda_n\right]_{n\in\mathbf{Z}} = S^{j+1} f_d * h \quad \text{then} \quad S^j f_d = \left[\lambda_{2n}\right]_{n\in\mathbf{Z}} . \tag{92}$$

The proof of this lemma is given in appendix 4. Lemma 3 shows that $W^j f_d$ can be computed by convolving $S^{j+1} f_d$ with the discrete filter g . To compute $S^j f_d$ we must convolve $S^{j+1} f_d$ with the discrete filter h and keep every other sample of the convolution product. By iterating on equations (91) and (92), it is now easy to decompose the discrete signal $S^0 f_d$ into the discrete wavelet transform $\left\{\left[W^j f_d\right]_{0>j\geq -J}, S^{-J} f_d\right\}$. This pyramidal algorithm is illustrated by a bloc diagram in Fig. 18. If $S^0 f_d$ has N non zero samples, each discrete signal $W^j f_d$ has approximatively $N2^{j+1}$ non zero samples and that $S^{-J} f_d$ will have $N2^{-J}$ non zero samples. The computational complexity of the algorithm is $N \log(N)$. The dyadic wavelet decomposition shown in Fig. 4 was computed with the coefficients of the filters h and g given in Fig. 16.

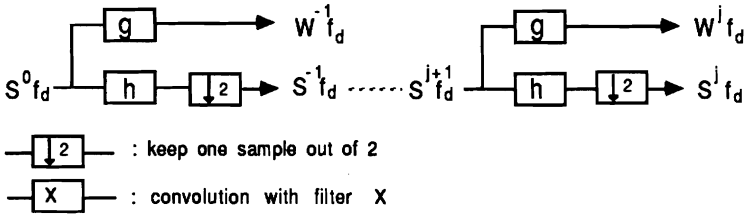

Fig. 18 *This bloc diagram illustrates the pyramidal architecture of the algorithm which decomposes the interpolated signal $S^0 f_d$ into a discrete wavelet representation. This algorithm is based on convolutions with the two filters h and g .*

To compute the EZC representation, we can then estimate the position of the zero-crossings with a linear interpolation between the samples of $W^j f_d$ which change sign. The energies between each pair of zero-crossings can also be estimated with a similar linear interpolation from the square of the samples.

6.2. Implementation of the reconstruction algorithm

We will now describe the numerical implementation of the reconstruction algorithm explained in paragraph 5.2. This reconstruction algorithm is based on two projection operators : $P_{\mathbf{F}}$ and $P_{\Gamma \mathbf{f}}$. We saw in paragraph 2.3.2 that the projection operator $P_{\mathbf{F}}$ could be decomposed into

$$P_{\mathbf{F}} = \mathbf{W}_{\mathbf{F}} \; o \; A^0 \; o \; \mathbf{W}_{\mathbf{F}}^{-1} \; . \tag{93}$$

The discrete implementation of the operator $\mathbf{W}_{\mathbf{F}}$ has been described in paragraph 6.1.3 . In the next paragraph we will explain another discrete pyramidal algorithm for implementing the inverse wavelet operator $\mathbf{W}_{\mathbf{F}}^{-1}$. We will then detail the implementation of the orthogonal projection operator A^0 and give a simple algorithm for computing the non linear projection on $\Gamma \mathbf{f}$.

6.2.1. Pyramidal implementation of a discrete inverse wavelet transform

A discrete wavelet operator transforms a uniform sampling $S^0 f_d$ of an approximated signal $S^0 f(x)$ into a discrete dyadic wavelet representation $\left\{ \left[W^j f_d \right]_{0 > j \geq -J} , S^{-J} f_d \right\}$. We will now describe another pyramidal algorithm for implementing a discrete version of the inverse wavelet transform $\mathbf{W}_{\mathbf{F}}^{-1}$. This operator reconstructs $S^0 f_d$ from $\left\{ \left[W^j f_d \right]_{0D > j \geq -J} , S^{-J} f_d \right\}$. The algorithm is based on a discretization of equation (51).

For each scale 2^j we are going to show how to compute $S^{j+1} f_d$ from the two discrete signals $S^j f_d$ and $W^j f_d$. The first step of this calculation consists of interpolating between each sample of $S^j f_d = \left[S^j f(n 2^{-j_0 - j + 1}) \right]_{n \in \mathbf{Z}}$ in order to get a sampling of $S^j f(x)$ at a rate $2^{j_0 + j} : \Lambda = \left[S^j f(n 2^{-j_0 - j}) \right]_{n \in \mathbf{Z}}$. This interpolation is computed with the spline function $\rho(x)$ described in paragraph 6.1.2.

$$\forall n \in \mathbf{Z} \; , \; S^j f((2n+1) 2^{-j_0 - j}) \approx \sum_{k=-\infty}^{+\infty} S^j f(k 2^{-j_0 - j + 1}) \, \rho(\frac{2n+1}{2} - k) \; . \tag{94}$$

Equation (91) shows that the intermediate sample $\left[S^j f((2n+1) 2^{-j_0 - j}) \right]_{n \in \mathbf{Z}}$ can be computed by putting a zero between each sample of $S^j f_d$ and convolving the resulting signal with the interpolation filter $\left[\rho(\frac{n}{2}) \right]_{n \in \mathbf{Z}}$. Fig. 19 gives the coefficients of this filter when $\rho(x)$ is a cubic spline polynomial. Such an interpolation is not exact but it provides a precise estimate of the intermediate samples. Indeed, the Nyquist rate of $S^j f(x)$ is approximatively 2^j . Since we already have a sampling of $S^j f(x)$ at the rate $2^{j_0 + j - 1}$ the function $S^j f(x)$ will vary very smoothly between two samples $n 2^{-j_0 - j + 1}$ and $(n+1) 2^{-j_0 - j + 1}$. The smoothness of $S^j f(x)$ is well approximated by the spline filter previously mentioned so equation (94) will give us a close estimation of the intermediate samples.

Let $\tilde{h} = \left[h_{-n} \right]_{n \in \mathbf{Z}}$ and $\tilde{g} = \left[g_{-n} \right]_{n \in \mathbf{Z}}$ be the symmetricals of the two filters h and g defined in (84). The following lemma shows that $S^{j+1} f_d$ can be computed by convolving $W^j f_d$ and Λ with the two filters $\tilde{g}$ and $\tilde{h}$.

Lemma 4

$$\text{Let} \quad \Lambda = \left[S^j f\left(n 2^{-j_0 - j} \right) \right]_{n \in \mathbf{Z}} , \quad S^{j+1} f_d = \Lambda * \tilde{h} + W^j f_d * \tilde{g} . \tag{95}$$

The proof of Lemma 4 is detailed in appendix 5. By repeating this reconstructing operation for $0 > j \geq -J$, we can reconstruct $S^0 f_d$ from the discrete wavelet representation $\left\{ \left[W^j f_d \right]_{0 < j \leq -J} , S^{-J} f_d \right\}$. The filters h and g that we used for our implementation are symmetrical so $\tilde{h} = h$ and $\tilde{g} = g$. The bloc diagram shown in Fig. 19 illustrates the pyramidal algorithm which implements a discrete inverse wavelet transform $\mathbf{W_F}^{-1}$.

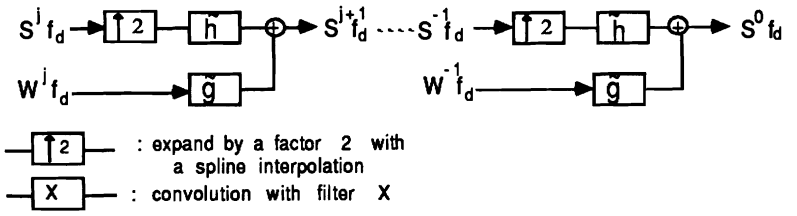

Fig. 19 *This bloc diagram illustrates the pyramidal algorithm for reconstructing the interplated signal $S^0 f_d$ from a discrete wavelet decomposition. This reconstruction is based on convolutions with the two discrete filters $\tilde{h}$ and $\tilde{g}$.*

As described in paragraph 2.3.2, in order to define the projection operator $P_{\mathbf{F}}$, $\mathbf{W_F}^{-1}$ must be extended to the whole space $(\mathbf{L}^2)^{j_2 - j_1}$. The discrete implementation of $\mathbf{W_F}^{-1}$ that we just described reconstructs $S^0 f_d$ from $\left\{ \left[W^j f_d \right]_{0 < j \leq -J} , S^{-J} f_d \right\}$. To implement the projection operator $P_{\mathbf{F}}$, we need to extend this algorithm to any sequence of discrete signals $\left[d_j \right]_{0 > j \geq J-1}$, where $d_j = \left[d_{n 2^{-j_1 - j}} \right]_{n \in \mathbf{Z}}$ is any sequence in $\mathbf{l}^2(\mathbf{Z})$. Let $d = \left[d_{n 2^{-j_1 + 1}} \right]_{n \in \mathbf{Z}}$ be the discrete signal which is obtained by applying the operator $\mathbf{W_F}^{-1}$ on $\left[d_j \right]_{0 > j \geq -J-1}$. Theorem 3 shows that this discrete signal can be considered as a uniform sampling at the rate $2^{j_0 - 1}$ of a function $d(x) \in \mathbf{V}_{j_0 - 1}$, where

$$d(x) = \sum_{n = -\infty}^{+\infty} d_{n 2^{-j_1 + 1}} \, 2^{-j_0 + 1} \, \rho^{j_0 - 1}(x - 2^{-j_0 + 1} n) . \tag{96}$$

For implementing the operator P_F, we must compute the orthogonal projection of $d(x)$ on the vector space $\mathbf{V}_0$. This orthogonal projection will be characterized by a uniform sampling at a rate 1 in order to apply afterwards the pyramidal wavelet algorithm described in paragraphs 6.1.2 and 6.1.3 .

6.2.2. Implementation of the projection operator A^0

The operator A^0 is an orthogonal projection from $\mathbf{L}^2$ on the vector space $\mathbf{V}_0$. In this paragraph, we are going to show how to compute the orthogonal projection on $\mathbf{V}_0$ of any function $d(x) \in \mathbf{V}_{j_0-1}$. The orthogonal projection $A^0 d(x)$ will be characterized by a uniform sampling at a rate 1 . Equation (36) implies that

$$A^0 d(x) = \sum_{p=-\infty}^{+\infty} < d(x) , \xi(x-p) > \xi(x-p) \quad . \tag{97}$$

The expression of d(x) given in equation (96) yields

$$< d(x) , \xi(x-p) > = \sum_{n=-\infty}^{+\infty} d_{n2^{-j_0+1}} 2^{-j_0+1} < \rho^{j_0-1}(u-2^{-j_0+1}n) , \xi(u-p) > \quad .$$

Each of the inner product $< \rho^{j_0-1}(u-2^{-j_0+1}n) , \xi(u-p) >$ can be expressed as a convolution product so that

$$< d(x) , \xi(x-p) > = \sum_{n=-\infty}^{+\infty} d_{n2^{-j_0+1}} 2^{-j_0+1} \ \rho^{j_0-1} * \xi(p-2^{-j_0+1}n) \quad .$$

The sequence of inner products $\left[< d(x) , \xi(x-p) > \right]_{p \in \mathbf{Z}}$ can thus be computed by convolving the sequence $\left[d_{n2^{-j_0+1}} \right]_{n \in \mathbf{Z}}$ with the discrete filter $\left[2^{-j_0+1} \ \rho^{j_0-1} * \xi(n2^{-j_0+1}) \right]_{n \in \mathbf{Z}}$ and keeping one sample out of 2^{-j_0+1} of the convolution product. The uniform sampling of $A^0 d(x)$ at a rate 1 is given by the sequence $\left[A^0 d(k) \right]_{k \in \mathbf{Z}}$. Equation (97) yields

$$A^0 d(k) = \sum_{p=-\infty}^{+\infty} < d(x) , \xi(x-p) > \xi(k-p) \quad .$$

This uniform sampling is therefore equal to the convolution of $\left[< d(x) , \xi(x-p) > \right]_{p \in \mathbf{Z}}$ with the filter $\left[\xi(n) \right]_{n \in \mathbf{Z}}$. In conclusion, equations (98) and (99) show that $\left[A^0 d(k) \right]_{k \in \mathbf{Z}}$ can be computed from the discrete signal $\left[d_{n2^{-j_0+1}} \right]_{n \in \mathbf{Z}}$ by :

- convolving $\left[d_{n2^{-j_0+1}} \right]_{n \in \mathbf{Z}}$ with the discrete filter $\left[2^{-j_0+1} \ \rho^{j_0-1} * \xi(n2^{-j_0+1}) \right]_{n \in \mathbf{Z}}$,
- taking one sample out of 2^{j_0-1} of the convolved signal,
- convolving the sub-sampled signal with the filter $\left[\xi(n) \right]_{n \in \mathbf{Z}}$.

The coefficients of the discrete filters $\left[c_n = 2^{-j_0+1}\,\rho^{j_0-1} * \xi(n\,2^{-j_0+1})\right]_{n\in Z}$ and $\left[\xi(n)\right]_{n\in Z}$ are given by Fig. 20 in the case of a cubic spline polynomial, for $j_0 = 3$.

n	c_n	n	c_n	n	c_n	n	c_n
0	0.272	4	-0.185	8	0.012	12	-0.006
1	0.237	5	-0.047	9	0.020	13	-0.009
2	0.153	6	-0.039	10	0.015	14	-0.006
3	0.056	7	-0.013	11	0.003	15	-0.001

n	$\xi(n)$	n	$\xi(n)$
0	1.089	4	0.013
1	-0.075	5	-0.006
2	0.047	6	0.003
3	-0.025	7	-0.002

Fig. 20 *Coefficients of the discrete filters* $\left[\xi(n)\right]_{n\in Z}$ *and* $\left[c_n = 2^{-j_0+1}\,\rho^{j_0-1} * \xi(n\,2^{-j_0+1})\right]_{n\in Z}$ *for* $j_0 = 3$, *in the case of a cubic spline polynomial. These filters are symmetrical.*

Equation (93) shows that the projection operator P_F can now be implemented by computing an inverse discrete wavelet transform W_F^{-1}, then an orthogonal projection A^0 on the vector space V_0 and, finally, a discrete wavelet transform W_F. In order to finish the implementation of the reconstruction algorithm described in paragraph 5.2, we must now define numerically the projection operator $P_{\Gamma f}$.

6.2.3. Implementation of a projection operator on Γf

By definition, a projection on Γf should verify the two properties (77) and (78). It must transform any sequence of curves $\left[g_j(x)\right]_{j_1-1\le j<j_2} \in (L^2)^Z$ into a new sequence of curves $\left[h_j(x)\right]_{j_1-1\le j<j_2} \in \Gamma f$. The function $h_{j_1-1}(x)$ should be equal to $S^{j_1}f(x)$ and for $j_1 \le j < j_2$ each function $h_j(x)$ should have the same energies and zero-crossings as $T^j f(x)$. We will describe a simple algorithm for implementing this deformation.

Let $j_1 \leq j < j_2$ and $\left[z_n^j\right]_{n\in\mathbf{Z}}$, $\left[e_n^j\right]_{n\in\mathbf{Z}}$ be respectively the positions of the zero-crossings and the energies of each function $T^j f(x)$. We are going to deform a function $g_j(x)$ into a function $h_j(x)$ whose zero-crossings and local energies will be equal to $\left[z_n^j\right]_{n\in\mathbf{Z}}$ and $\left[e_n^j\right]_{n\in\mathbf{Z}}$. This deformation is illustrated by Fig. 21. We first define a function $\alpha(x)$ such that for each pair of consecutive zeros (z_{n-1}^j , z_n^j)

$$\forall x \in [z_{n-1}^j , z_n^{j-1}] \quad , \quad \alpha(x) = g_j(x) - a\,x + b \quad \text{with} \quad \begin{cases} a\, z_{n-1}^j + b = -g_j(z_{n-1}^j) \\ a\, z_n^j + b = -g_j(z_n^j) \end{cases} . \tag{100}$$

The function $\alpha(x)$ has a zero-crossing at each point $\left[z_n^j\right]_{n\in\mathbf{Z}}$ but might have some other ones (see Fig. 21). We need to remove these spurious zero-crossings and keep the sign of $\alpha(x)$ constant and equal to the sign of e_n^j on each interval $]z_{n-1}^j , z_n^{j-1}[$. This operation is done in the following loop. In this loop we add a triangle function to $\alpha(x)$ to suppress the regions of $]z_{n-1}^j , z_n^{j-1}[$ where $\alpha(x)$ has a sign different than the sign of e_n^j (see Fig. 21).

While $\alpha(x)$ has a zero-crossing in the interval $]z_{n-1}^j , z_n^{j-1}[$:

let $x_n \in]z_{n-1}^j , z_n^{j-1}[$ be such that $\alpha(x_n)\, sign(e_n^j) = \min_{x \in]z_{n-1}^j , z_n^{j-1}[} \{ \alpha(x)\, sign(e_n^j) \}$,

for $x \in [z_{n-1}^j , x_n]$, $\alpha(x) = \alpha(x) - 2\,\alpha(x_n)\, \dfrac{x - z_{n-1}^j}{x_n - z_{n-1}^j}$,

for $x \in [x_n , z_n^j]$, $\alpha(x) = \alpha(x) - 2\,\alpha(x_n)\, \dfrac{x - z_n^j}{x_n - z_n^j}$,

end of loop.

Let us call $\beta(x)$ the function $\alpha(x)$ which is obtained at the end of this loop. On each interval $[z_{n-1}^j , z_n^{j-1}]$, the sign of $\beta(x)$ is equal to the sign of e_n^j and $\beta(z_{n-1}^j) = \beta(z_n^j) = 0$. We must now dilate $\beta(x)$ on each of these interval in order to have a local energy equal to e_n^j . The function $h_j(x)$ is thus defined by :

$$\forall n \in \mathbf{Z} \quad , \quad \forall x \in [z_{n-1}^j , z_n^{j-1}] \quad , \quad h_j(x) = \frac{e_n^j\, \beta(x)}{\left[\int_{z_{n-1}^j}^{z_n^j} \beta(x)^2\, dx \right]^{1/2}} . \tag{101}$$

The overall deformation process is illustrated in Fig. 21. One can easily verify that such a deformation defines a projection operator $P_{\Gamma f}$ which verifies equations (77) and (78).

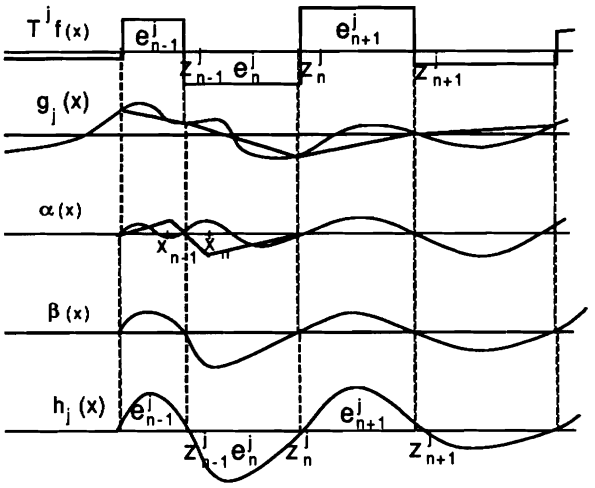

Fig. 21 *Illustration of the deformation algorithm for implementing the projection operator* $P_{\Gamma f}$. *The function* $g_j(x)$ *is deformed in order to match its zero-crossings and local energy values with the zero-crossings and local energy values of* $T^j f(x)$.

7. Application of the EZC representation to stereo matching

An important problem in computer vision is to recover a three dimensional description of the surfaces which appear in a scene. From two images of a single scene, one can indeed compute the distance between each point of the scene and the pair of stereo cameras. Let P be a point of the world which is projected on both images. Let P_l and P_r be respectively the projections of P on the left and the right images (see Fig. 22). One can compute the distance from P to the pair of stereo cameras from the difference of positioning τ between P_l and P_r (see Fig. 22). This difference of positioning is called a disparity. The goal of a stereo-matching algorithm is to find for each point P_l of the left image, the matching point P_r of the right image such that P_l and P_r are the projections of the same point P of the scene. The principle of such an algorithm is to look for a point P_r in the right image such that locally around P_r the image is the most similar to the neighborhood around P_l in the left image. Although this matching problem is a priori a two dimensional search, it can be reduced to a one dimensional search by using the epipolar geometry of the cameras (see Fig. 22). An epipolar plane is a plane which contains the point P and the optical centers of the left and right cameras. The intersections of such a plane with the left and the right images define a pair of epipolar lines. The stereo match of any point which is on a left epipolar line can be found on the corresponding right epipolar line. The problem is thus reduced to a one dimensional matching problem along each pair of epipolar lines. Much research has been devoted to finding efficient algorithms for

matching these epipolar lines [7, 18]. We will show that such an algorithm can easily be implemented with the EZC representation.

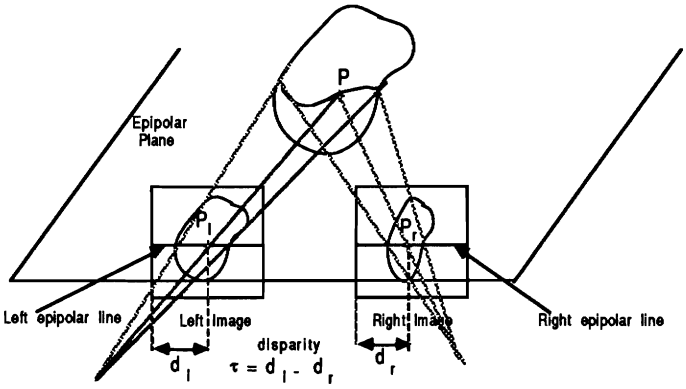

Fig. 22 *Example of horizontal epipolar geometry of a pair of stereo images. A point P of the scene appears respectively in P_l and P_r in the left and right images.*

7.1. Matching Algorithm

Let us suppose that our left and right images have N^2 pixels each. A left and right epipolar scan line will have N samples each : $\left[l_n\right]_{1\le n<N}$ and $\left[r_n\right]_{1\le n<N}$. Each of these sequences of samples characterize the approximation of a signal at the resolution 1. Let $S^0l(x)$ and $S^0r(x)$ be respectively the left and right approximated signals which interpolate these samples. For every point x_0, the goal of the matching process is to find the disparity $\tau(x_0)$ such that $S^0l(x_0)$ and $S^0r(x_0-\tau(x_0))$ are locally the most similar. For this purpose, we will compute the finite EZC representations of $S^0l(x)$ and $S^0r(x)$ and compare locally these two representations with a coarse to fine strategy. A coarse to fine strategy consists of matching first the coarser details of the two signals $S^0l(x)$ and $S^0r(x)$ and then using the finer details to get more precise matches. Let $\left\{\left[T^jl(x)\right]_{-J\le j\le-1}, S^{-J}l(x)\right\}$ and $\left\{\left[T^jr(x)\right]_{-J\le j\le-1}, S^{-J}r(x)\right\}$ be respectively the finite EZC representation of the left and the right approximated signals between the scales 1 and 2^{-J}. We have described in paragraph 6.1 how to compute these representations given the sequences of samples $\left[l_n\right]_{1\le n<N}$ and $\left[r_n\right]_{1\le n<N}$. Matching two signals $T^jl(x)$ and $T^jr(x)$ consists of trying to match their zero-crossings. We will use the local distance defined by equation (75) for matching the zero-crossings around which $T^jl(x)$ and $T^jr(x)$ are the most similar. Let $\left[z_k^j\right]_{j\in\mathbf{Z}}$, $\left[e_k^j\right]_{j\in\mathbf{Z}}$ and $\left[\bar{z}_k^j\right]_{j\in\mathbf{Z}}$, $\left[\bar{e}_k^j\right]_{j\in\mathbf{Z}}$ be respectively the zero-crossings and energies of $T^jl(x)$ and $T^jr(x)$. Given a zero-crossing z_k^j of $T^jl(x)$ we want to find the zero-crossing $\bar{z}_p^j$ of $T^jr(x)$ such that if

$\tau = z_k^j - \bar{z}_p^j$ then

$$\mathbf{d}_{z_k^j}^j(\mathbf{T_F} l(x)\,,\,\mathbf{T_F} r(x-\tau)) = \left[\int_{z_k^j - 2^{-j}\sigma}^{z_k^j + 2^{-j}\sigma} (T^j l(x) - T^j r(x-\tau)^2\, dx \right]^{1/2} = d_{\min} \quad \text{is minimum} \ . \qquad (102)$$

This means that the neighborhood of $T^j r(x)$ around $\bar{z}_p^j$ is the most similar to the neighborhood of $T^j l(x)$ around z_k^j (see Fig. 25). This minimum value $d_{\min}$ gives also a confidence measure on the match. The smaller $d_{\min}$ is, the higher our confidence in the match. Each match between a zero-crossing of $T^j l(x)$ and a zero-crossing of $T^j r(x)$ gives a local estimate of the disparity τ. At the next scale 2^{j+1} we will use this local estimate of the disparity in order to constrain the search when trying to find the correspondence between the zero-crossings of $T^{j+1} l(x)$ and the zero-crossings of $T^{j+1} r(x)$. When beginning at the coarser scale 2^{-J} we do not have any prior estimation of the disparity to constraint the search. This is, however, not a problem since the number of zero-crossings of $T^{-J} l(x)$ and $T^{-J} r(x)$ will be small when J is big enough (see Fig. 25).

7.2. Discussion of the algorithm and results

The coarse to fine strategy reduces considerably the complexity of the search for a match since we use the matching information at the previous scale to constrain the search at the next scale. This strategy presupposes that we have a good confidence in the matches at the coarser scales since any error at a coarse scale might propagate at finer scales. At the coarse level we have a higher confidence in the matches because the signals $T^j l(x)$ and $T^j r(x)$ have less distortions (see Fig. 24). Indeed, the distortions between the left and right epipolar signals are primarily introduced in the high frequencies of these signals. The distortions are due to the difference of viewing perspective, to the camera system's noise and to the errors on the positioning of the epipolar lines in the two images. The matches at the coarser scales will thus be more reliable.

In order to avoid side effects, at each scale, we did not try to to match the zero-crossings at the borders. As we can see from the successive matchings shown in Fig. 25 , we are getting a very dense matching on the signal. There are, however, some domains of the signal where we do not match the zero-crossings because there is too much distortion between $T^j l(x)$ and $T^j r(x)$. In these domains, the minimal distance $d_{\min}$ of any pair of matching zero-crossings will be large. We have included in our algorithm a confidence threshold c_0 in order to eliminate such matches. If $\frac{1}{d_{\min}} < c_0$ we eliminate the match. As shown in Fig. 25, in some domains we are able to find some matches at a coarse scale but not at finer scales because there is too much high frequency noise. By comparing Fig. 23 and Fig. 24, we can see that when the left and right signal are locally similar, at each scale $T^j l$ and $T^j r$ are also similar. It is very rare that the discontinuity of the operator $\mathbf{T_F}$, mentioned in paragraph

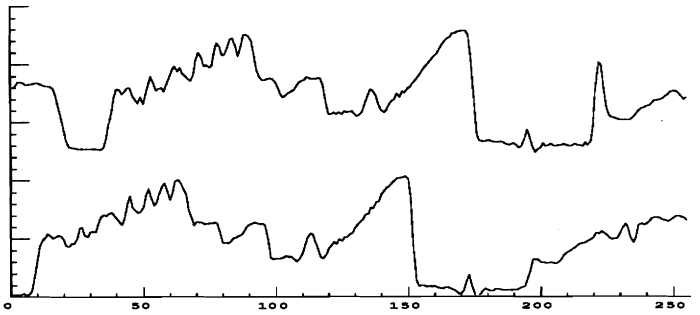

Fig. 23 *Pair of stereo epipolar scan lines from a real pair of stereo images. The distortion between these two signals is due to the difference of viewing perspective, to the camera noise and to the errors in the computation of the epipolar geometry.*

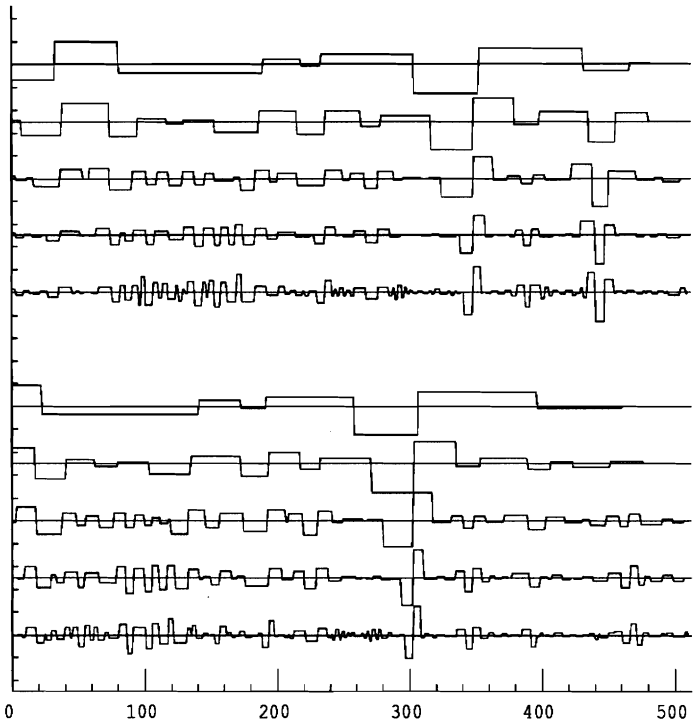

Fig. 24 *Energy Zero-Crossing representations of the two epipolar lines. The top EZC representation corresponds to the left signal and the bottom one to the right signal. We want to match these representations with a coarse to fine strategy.*

5.3, introduces a noticeable perturbation. As explained in paragraph 5.1 , the distance $\mathbf{d}_{z_i}^{j}$ which must be minimized is simple to compute.

As a conclusion we would like to emphasize that such a stereo-matching algorithm is very simple to develop because the EZC representation in itself is well adapted to this pattern recognition problem. We did not try to add

any verification procedure on the matches obtained with this algorithm because our goal was just to demonstrate the efficiency of the representation.

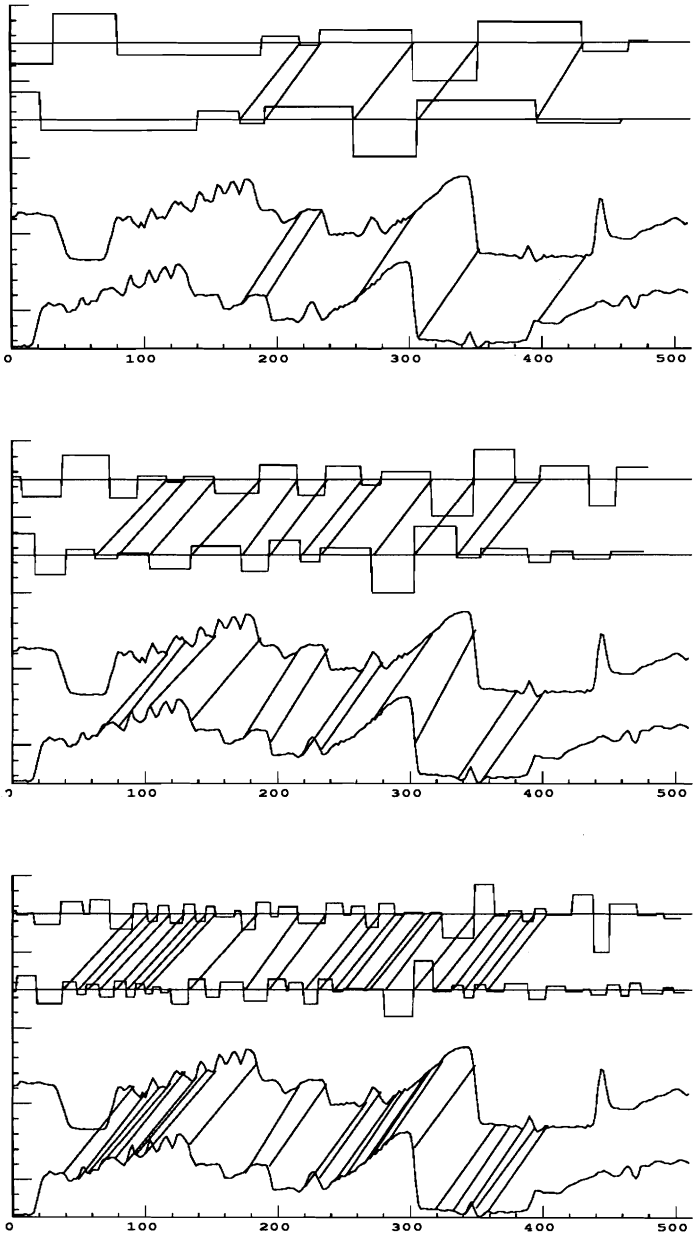

Fig. 25. *Coarse to fine matching between the zero crossings at the resolutions* 2^{-5} , 2^{-4} *and* 2^{-3} *of the EZC representations of a pair of stereo epipolar lines.*

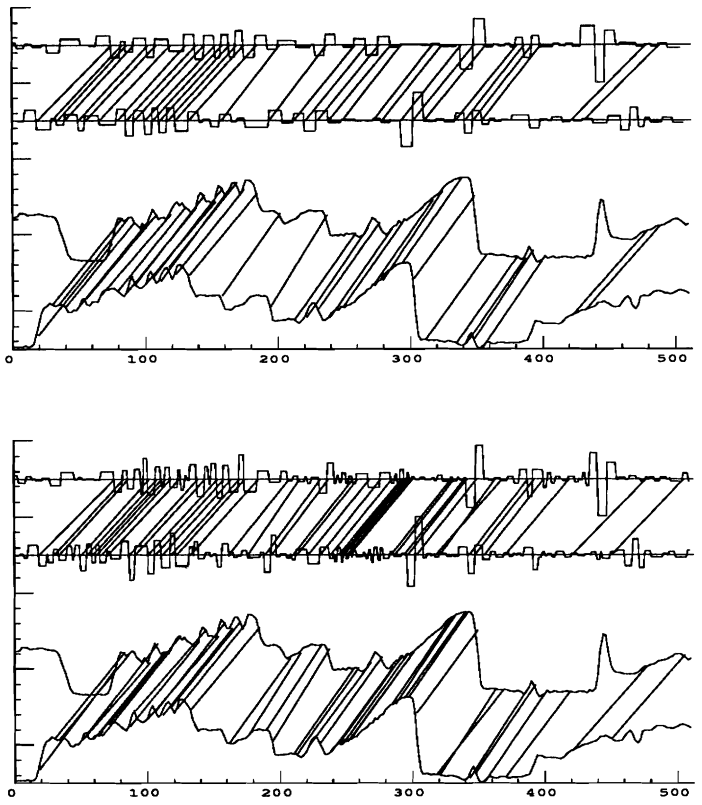

Fig. 25. *Coarse to fine matching between the zero crossings at the resolutions* 2^{-2} *and* 2^{-1} *of the EZC representations of a pair of stereo epipolar lines.*

8. Conclusion

In this paper we have defined a general low-level signal representation for signal analysis. This representation is based upon the position of the zero-crossings of the dyadic wavelet representation and the values of the local energy between each pair of zero-crossings. We have first studied the mathematical properties of a dyadic wavelet representation and have then derived the properties of the Energy Zero-Crossing representation. The EZC representation is (experimentally) complete and admits a simple metric for pattern recognition applications. It has a multiscale organization and provides the locations of the signal "edges" at each scale. We have described a recursive algorithm for reconstructing a signal from its EZC representation. The convergence of the algorithm gives an experimental proof of the completeness of this representation. However, the mathematical proof remains an open problem. We have described the numerical implementation of all our algorithms. We have shown in particular that we could implement a discrete wavelet transform with a pyramidal algorithm of complexity n.log(n) .

A similar algorithm has been described for implementing a discrete inverse wavelet transform. We have developed a coarse to fine stereo-matching algorithm to illustrate the application of this decomposition to pattern recognition. The simplicity and the efficiency of this matching algorithm shows that the EZC representation is indeed well adapted for pattern recognition problems.

Acknowledgments

I would to like to thank particularly Ruzena Bajcsy for her guidance throughout this research. I am also very grateful to Ingrid Daubechies with whom I have studied the discontinuity of the Energy Zero-Crossing representation and to Philippe Tchamitchian who suggested me the defintion of a dyadic wavelet transform.

Appendix 1

This appendix gives a proof of Lemma 1. We have already shown that if $\psi(x)$ is a wavelet, it must verify the conditions of Lemma 1. Conversely, let $\psi(x)$ be a function verifying the condition of the lemma. Let $\hat{\phi}(\omega)$ be a function defined by $\hat{\phi}(\omega) \geq 0$ and

$$|\hat{\phi}(\omega)|^2 = \sum_{j=1}^{+\infty} |\hat{\psi}(2^j \omega)|^2 \quad . \tag{103}$$

The functions $\hat{\phi}(\omega)$ and $\hat{\psi}(\omega)$ verify

$$|\psi(\omega)|^2 = |\hat{\phi}(\frac{\omega}{2})|^2 - |\hat{\phi}(\omega)|^2 \quad .$$

In order to prove that $\psi(x)$ is a wavelet we will show that $\hat{\phi}(\omega)$ is the Fourier transform of a scaling function. Let us prove first that $\hat{\phi}(\omega)$ is sqare integrable :

$$\int_{-\infty}^{+\infty} |\hat{\phi}(\omega)|^2 \, d\omega = \int_{-\infty}^{+\infty} \sum_{j=1}^{+\infty} |\hat{\psi}(2^j \omega)|^2 \, d\omega = 2\pi \sum_{j=1}^{+\infty} 2^{-j} ||\psi||^2 = 2\pi \quad .$$

The function $\hat{\phi}(\omega)$ is thus a square integrable function. It defines the Fourier transform of a function $\phi(x)$ and with Parseval's theorem we can derive that $||\phi|| = 1$. By scaling equation (103) by 2^J we get

$$\forall \omega \in \mathbf{R} \quad , \quad |\hat{\phi}(2^J \omega)|^2 = \sum_{j=J}^{+\infty} |\hat{\psi}(2^j \omega)|^2 \quad .$$

From the uniform convergence of $\sum_{j=J}^{+\infty} |\hat{\psi}(2^j \omega)|^2$ when J goes to $+\infty$ we can easily derive that

$$\lim_{|\omega| \to 0} |\hat{\phi}(\omega)| = 1 \quad \text{and}$$

$$\lim_{|\omega| \to +\infty} |\hat{\phi}(\omega)| = 0 \quad .$$

Since $\hat{\phi}(\omega) \geq 0$ it will thus verify the limit conditions (10) and (11) of a smoothing function. Finally, $\hat{\phi}(\omega)$ clearly verifies the causality condition of a smoothing function since

$$|\hat{\phi}(2\omega)|^2 = \sum_{j=2}^{+\infty} |\hat{\psi}(2^j \omega)|^2 \leq |\hat{\phi}(\omega)|^2 \quad .$$

The inverse Fourier transform of $\hat{\phi}(\omega)$ is thus a smoothing function. This concludes the proof of lemma 1.

Appendix 2

This appendix gives a proof to Lemma 2 and shows that the inverse is not true. In order to simplify the proof we will choose $j = 0$. It can then be easily extended for any $j \in \mathbf{Z}$. By taking the Fourier transform of equation (37), we can show that the Fourier transform of any function $f^*(x) \in \mathbf{V}_0$ is given by

$$\hat{f}^*(\omega) = \hat{\xi}(\omega) \sum_{n=-\infty}^{+\infty} \alpha_n \, e^{-in\omega} \; . \tag{104}$$

Equation (38) shows that $f^*(\omega)$ can be written

$$\hat{f}^*(\omega) = \hat{\phi}(\omega)\hat{f}(\omega) \qquad \text{where} \quad \hat{f}(\omega) = \hat{v}(2^{-j}\omega) \sum_{n=-\infty}^{+\infty} \alpha_n \, e^{-in\omega} \; . \tag{105}$$

In order to prove equation (39) we must show that $\hat{f}(\omega) \in \mathbf{L}^2$. Let us compute the integral of $|f(\omega)|^2$:

$$\int_{-\infty}^{+\infty} |\hat{f}(\omega)|^2 \, d\omega = \sum_{k=-\infty}^{+\infty} \int_{k2\pi}^{(k+1)2\pi} |\hat{f}(\omega)|^2 \, d\omega = \sum_{k=-\infty}^{+\infty} \int_{k2\pi}^{(k+1)2\pi} \Big| \sum_{n=-\infty}^{+\infty} \alpha_n \, e^{-in\omega} \Big|^2 \, |v(\omega)|^2 \, d\omega \; .$$

Since $\sum_{n=-\infty}^{+\infty} \alpha_n \, e^{-in\omega}$ is 2π periodic, and since we know that $\exists C > 0$ such that $|v(\omega)|^2 < \frac{C}{1+\omega^2}$, we have

$$\int_{-\infty}^{+\infty} |\hat{f}(\omega)|^2 \, d\omega = \int_{0}^{2\pi} \Big| \sum_{n=-\infty}^{+\infty} \alpha_n \, e^{-in\omega} \Big|^2 \sum_{k=-\infty}^{+\infty} |v(\omega + k2\pi)|^2 \le \sum_{n=-\infty}^{+\infty} |\alpha_n|^2 \sum_{k=-\infty}^{+\infty} \frac{C}{(1+2k\pi)^2} \; .$$

This equation shows that $\hat{f}(\omega)$ is square integrable. It thus defines the Fourier transform of a function $f(x) \in \mathbf{L}^2$ and $f^*(x) = S^0 f(x)$. This concludes the proof of lemma 2.

Conversely, not every function $f(x) \in \mathbf{L}^2$ verifies $S^j f(x) \in \mathbf{V}_j$. In order to verify such a property, the Fourier transform of f(x) must be given by equation (105). The inverse Fourier transform of this equation can be written

$$f(x) = \sum_{n=-\infty}^{+\infty} \alpha_n \, v(x-n) \; .$$

The function f(x) must therefore be in the vector space generated by the family of functions $\Big[v(x-n) \Big]_{n \in \mathbf{Z}}$.

Appendix 3

This appendix gives the proof of theorem 3. This Lemma will be proved for $j = 0$ since we can then generalized the result for any $j \in \mathbf{Z}$ by scaling the functions $\xi(x)$ and $\rho(x)$ by a factor 2^j . Let us write equation (43) for $f(x) = \xi(x)$,

$$\xi(x) = \sum_{n=+\infty}^{-\infty} \xi(n)\, \rho(x-n) \ . \tag{106}$$

If we take the Fourier transform of this equation, by applying the Poisson formula we get

$$\hat{\xi}(\omega) = \sum_{n=-\infty}^{+\infty} \hat{\xi}(\omega + 2n\pi)\ \hat{\rho}(\omega) \ . \tag{107}$$

The Fourier transform of $\rho(x)$ must therefore verify

$$\hat{\rho}(\omega) = \frac{\hat{\xi}(\omega)}{\sum_{n=-\infty}^{+\infty} \hat{\xi}(\omega + 2n\pi)} \ . \tag{108}$$

This equation defines a function in $\mathbf{L}^2$ since $c_2 \geq \sum_{n=-\infty}^{+\infty} \hat{\xi}(\omega + 2n\pi) \geq c_1$.

Let us now suppose that $\rho(x)$ is a function whose Fourier transform is defined by equation (108) . We are going to prove that the property (43) is indeed verified. Since $\sum_{n=-\infty}^{+\infty} \hat{\rho}(\omega + 2n\pi) = 1$ by applying the Poisson formula we can easily derive that

$$\forall n \in \mathbf{Z} \quad \rho(n) = \begin{cases} 1 & \text{if} \quad n = 0 \\ 0 & \text{if} \quad n \neq 0 \end{cases} \ . \tag{109}$$

By reversing the derivation steps of equation (106) and (107) we can show also that

$$\xi(x) = \sum_{n=+\infty}^{-\infty} \xi(n)\, \rho(x-n) \ .$$

From this equation, it is clear that for any $k \in \mathbf{Z}$ the function $\xi(x-k)$ can be decomposed on the family of functions $\left[\rho(x-n)\right]_{n \in \mathbf{Z}}$. Since $\left[\xi(x-k)\right]_{k \in \mathbf{Z}}$ is a basis of $\mathbf{V}_0$, any function $f(x) \in \mathbf{V}_0$ can thus be decomposed in the family of the functions $\left[\rho(x-n)\right]_{n \in \mathbf{Z}}$:

$$\exists (\alpha_n)_{n \in \mathbf{Z}} \quad , \quad f(x) = \sum_{n=+\infty}^{-\infty} \alpha_n\, \rho(x-n) \ .$$

Since $\rho(x)$ verifies the property (109) , for all $n \in \mathbf{Z}$ $\alpha_n = f(n)$. This concludes the proof of the theorem .

Appendix 4

In this appendix we give a proof of lemma 3.

Proof of equation (91): Let $\hat{W^j f_d}(\omega)$ be the Fourier series of the discrete signal $W^j f_d$ defined by equation (89) :

$$\hat{W^j f_d}(\omega) = \sum_{n \in Z} W^j f(n 2^{-j_0-j}) \, e^{-in 2^{-j_0-j} \omega} \, . \tag{110}$$

Since $W^j f(n 2^{-j_0-j}) = f * \psi^j(n 2^{-j_0-j})$, by applying the Poisson formula we can easily derive that

$$\hat{W^j f_d}(\omega) = \hat{f}(\omega) \, \hat{\psi}(2^{-j} \omega) * 2^{j_0+j} \sum_{n \in Z} \delta(\omega + n 2\pi 2^{j_0+j}) \quad \text{so}$$

$$\hat{W^j f_d}(\omega) = 2^{j_0+j} \sum_{n \in Z} \hat{f}(\omega + n 2\pi 2^{j_0+j}) \, \hat{\psi}(2^{-j} \omega + n 2\pi 2^{j_0}) \, . \tag{11}$$

Equation (13) yields

$$\hat{\psi}(2^{-j} \omega + n 2\pi 2^{j_0}) = G(2^{-j-1}\omega + n \pi 2^{j_0}) \, \hat{\phi}(2^{-j-1}\omega + n \pi 2^{j_0}) \, .$$

Since $G(\omega)$ is $2^{j_0}\pi$ periodic,

$$\hat{W^j f_d}(\omega) = 2^{j_0+j} \, G(2^{-j-1}\omega) \sum_{n \in Z} \hat{f}(\omega + n 2\pi 2^{j_0+j}) \, \hat{\phi}(2^{-j-1}\omega + n \pi 2^{j_0}) \, . \tag{112}$$

Let us now define the Fourier series $\hat{S^j f_d}(\omega)$ of the discrete signal $S^j f_d$.

$$\hat{S^j f_d}(\omega) = \sum_{n \in Z} S^j f(n 2^{-j_0-j+1}) \, e^{-i 2^{-j_0-j+1} n \omega} \, .$$

Since $S^j f(n 2^{-j_0-j+1}) = f * \phi^j(n 2^{-j_0-j+1})$, we can show similarly that $\hat{S^j f_d}(\omega 2^{-j_0-j+1})$ can be written

$$\hat{S^j f_d}(\omega) = 2^{j_0+j-1} \sum_{n \in Z} \hat{f}(\omega + n \pi 2^{j_0+j}) \, \hat{\phi}(2^{-j} \omega + n \pi 2^{j_0}) \, . \tag{113}$$

By comparing equation (112) and equation (114) we can now derive that

$$\hat{W^j f_d}(\omega) = G(2^{-j-1}\omega) \, \hat{S^{j+1} f_d}(\omega) \, . \tag{115}$$

This equation is the Fourier transform of the discrete convolution given in assertion (91) of lemma 3. This concludes the proof of equation (91) .

Proof of equation (92) : We saw in equation (114) that the Fourier series $\hat{S^j f_d}(\omega 2^{-j_0-j+1})$ can be written

$$\hat{S^j f_d}(\omega) = 2^{j_0+j-1} \sum_{n \in Z} \hat{f}(\omega + n \pi 2^{j_0+j}) \, \hat{\phi}(2^{-j} \omega + n \pi 2^{j_0}) \, .$$

We can derive from equation (7) that

$$\hat{\phi}(2^{-j}\omega + n\pi 2^{j_0}) = H(2^{-j-1}\omega + n\pi 2^{j_0-1})\ \hat{\phi}(2^{-j-1}\omega + n\pi 2^{j_0-1}) \quad \text{so}$$

$$\hat{S^j} f_d(\omega) = 2^{j_0+j-1} \sum_{n\in Z} \hat{f}(\omega + n\pi 2^{j_0+j})\, H(2^{-j-1}\omega + n\pi 2^{j_0-1})\, \hat{\phi}(2^{-j-1}\omega + n\pi 2^{j_0-1}) \ .$$

This summation can be divided in two for n even and n odd :

$$\hat{S^j} f_d(\omega) = 2^{j_0+j-1} \sum_{n\in Z} \hat{f}(\omega + n\pi 2^{j_0+j+1})\, H(2^{-j-1}\omega + n\pi 2^{j_0})\, \hat{\phi}(2^{-j-1}\omega + n\pi 2^{j_0}) +$$
$$2^{j_0+j-1} \sum_{n\in Z} \hat{f}(\omega + n\pi 2^{j_0+j+1} + \pi 2^{j_0+j})\, H(2^{-j-1}\omega + n\pi 2^{j_0} + \pi 2^{j_0-1})\, \hat{\phi}(2^{-j-1}\omega + n\pi 2^{j_0} + \pi 2^{j_0-1}) \ .$$

Since H is a $2^{j_0}\pi$ periodic function, this expression can be written

$$\hat{S^j} f_d(\omega) = H(2^{-j-1}\omega)\, 2^{j_0+j-1} \sum_{n\in Z} \hat{f}(\omega + n\pi 2^{j_0+j+1})\, \hat{\phi}(2^{-j-1}\omega + n\pi 2^{j_0}) +$$
$$H(2^{-j-1}\omega + \pi 2^{j_0-1})\, 2^{j_0+j-1} \sum_{n\in Z} \hat{f}(\omega + n\pi 2^{j_0+j+1} + \pi 2^{j_0+j})\, \hat{\phi}(2^{-j-1}\omega + n\pi 2^{j_0} + \pi 2^{j_0-1}) \ .$$

By comparing this equation with the expression of $\hat{S^j} f_d(\omega)$ given in equation (114) , we can derive that

$$\hat{S^j} f_d(\omega) = H(2^{-j-1}\omega)\, \hat{S^{j+1}} f_d(\omega) + H(2^{-j-1}\omega + \pi 2^{j_0-1})\, \hat{S^{j+1}} f_d(\omega + \pi 2^{j_0+j}) \ .$$

This expression is the Fourier transform of equation (92). It shows that $S^j f_d$ can be computed by convolving $S^{j+1} f_d$ with the discrete filter h and taking one sample out of two from the resulting discrete signal.

Appendix 5

In this appendix we give a proof to Lemma 4.

Proof of equation (95) : We saw in equation (115) of appendix 4 that

$$\hat{W}^j f_d(\omega) = G(2^{-j-1}\omega)\, \hat{S}^{j+1} f_d(\omega) \ .$$

Let $\hat{\Lambda}(\omega)$ be the Fourier series of the discrete signal Λ defined in equation (95) ,

$$\hat{\Lambda}(\omega) = \sum_{n \in \mathbf{Z}} S^j f\,(n 2^{-j_0-j})\, e^{-in 2^{-j_0-j}\omega} \ .$$

With a proof similar to the proof of equation (115) given in appendix 4, we can show that

$$\hat{\Lambda}(\omega) = H(2^{-j-1}\omega)\, \hat{S}^{j+1} f_d(\omega) \ .$$

Let $\overline{H}(2^{-j-1}\omega)$ and $\overline{G}(2^{-j-1}\omega)$ be respectively the complex conjugate of $H(2^{-j-1}\omega)$ and $G(2^{-j-1}\omega)$.

$$\overline{H}(2^{-j-1}\omega)\ \hat{\Lambda}(\omega) + \overline{G}(2^{-j-1}\omega)\ \hat{W}^j f_d(\omega) = (\ |H(2^{-j-1}\omega)|^2 + |G(2^{-j-1}\omega)|^2\ )\, \hat{S}^{j+1} f_d(\omega) \ .$$

$G(\omega)$ verifies $|H(\omega)|^2 + |G(\omega)|^2 = 1$ hence

$$\overline{H}(2^{-j-1}\omega)\ \hat{\Lambda}(\omega) + \overline{G}(2^{-j-1}\omega)\ \hat{W}^j f_d(\omega) = \hat{S}^{j+1} f_d(\omega) \ .$$

This equation is the Fourier transform of equation (95). This concludes the proof of lemma 4.

References

1. Crowley, J., "A representation for visual information," *Tech. Rep. CMU-RI-TR-82-7*, Robotic Inst. Carnegie-Mellon Univ., 1987.

2. Daubechie, I., "Othonormal bases of compactly supported wavelets," *subm. to IEEE Trans. on Information Theory*, Bell lab., 1987.

3. Daubechie, I., "The wavelet transform, time-frequency localization and signal analysis," *To appear in Commumications in pure and applied mathematics*, 1988.

4. Daubechie, I., Grossmann, A., and Meyer, Y., "Painless non-orthogonal expansions," *J. Math. Phys.* , vol. 27, pp. 1271-1283, 1986.

5. Federbush, P., "Quantum field theory in ninety minutes," *Bull. Am. Math. Soc.*, 1987.

6. Goupillaud, P., Grossmann, A., and Morlet, J., "Cycle octave and related tranform in seismic signal analysis," *Geoexploration* , vol. 23, pp. 85-102, 1985/84.

7. Grimson, W., "Computational experiments with a feature based stereo algorithm," *IEEE Trans. Pattern Analys. Machine Intell.*, vol. 7, pp. 17-34, Jan. 1985.

8. Grossmann, A. and Morlet, J., "Decomposition of Hardy functions into square integrable wavelets of constant shape," *SIAM J. Math.*, vol. 15, pp. 723-736, 1984.

9. Hummel, R., "Representations based on zero-crossings in scale-space," Tech. Rep. 225, Courant Inst., Dept. Computer Sc., June, 1986.

10. Hummel, R. and Moniot, R., "A network approach to reconstruction from zero-crossings," *Proc. of IEEE Workshop on computer vision.*

11. Jaffard, S. and Meyer, Y., "Bases d'ondelettes dans des ouverts de Rn," *Journ. de Mathematiques pures et appliquees*, 1987.

12. Kronland-Martinet, R., Morlet, J., and Grossmann, A., "Analysis of sound patterns through wavelet transform," *International Journal on Pattern Analysis and Artificial Intelligence*, Jan. 1987.

13. Lemarie, P.G., "Ondelettes a localisation exponentielles," *Journ. de Math. Pures et Appl.*. to be published

14. Lemarie, P. G. and Y., Meyer, "Ondelettes et bases hilbertiennes," *Revista Matematica Ibero Americana*, vol. 2, 1986.

15. Logan, B., "Information in the zero-crossings of band pass signals," *Bell Systems Tech. Journ.* , vol. 56, p. 510, 1977.

16. Mallat, S., "A theory for multiresolution signal decomposition : the wavelet representation," Tech. Rep. MS-CIS-87-22, U. of Penn., May 1987. Subm. to IEEE trans. on Pattern Analysis and Machine Intelligence.

17. Mallat, S., "Multiresolution approximation and wavelets," *Tech. Rep. MS-CIS-87-87*, U. of Penn, Aug. 1987. Subm. to Transactions of the Americain Mathematical Society.

18. Marr, D. and Poggio, T., "A theory of human stereo vision," *Proc. Royal Soc. London*, vol. B 204, pp. 301-328, 1979.

19. Meyer, Y., "Principe d'incertitude, bases hilbertiennes et algebres d'operateurs," *Bourbaki seminar*, 1985-86, no 662.

20. Sanz, J. and Huang, T., "Theorem and experiments on image reconstruction from zero-crossings," *Research report RJ5460* , IBM.

21. Witkin, A., "Scale space filtering," *Proc. Int. Joint Conf. Artificial Intell.* , 1983.

22. Yuille, A. and Poggio, T., "Scaling theorems for zero crossings," *IEEE trans on PAMI*, vol. 8, Jan 1986.

23. Zeevi, Y. and Rotem, D., "Image reconstruction from zero-crossings," *IEEE ASSP*, vol. 34, pp. 1269-1277, 1986.